Available online at www.sciencedirect.com
SCIENCE DIRECT®
Journal of Theoretical Biology 231 (2004) 413–433
Journal of Theoretical Biology
www.elsevier.com/locate/yjtbi

Estimation of neurophysiological parameters from the waking EEG using a biophysical model of brain dynamics

Donald. L. Rowe[a,b,*], Peter. A. Robinson[a,b], Christopher. J. Rennie[a,b,c]

[a]School of Physics, University of Sydney, New South Wales 2006, Australia
[b]The Brain Dynamics Centre, Westmead Hospital and University of Sydney, Westmead, New South Wales 2145, Australia
[c]Department of Medical Physics, Westmead Hospital, New South Wales 2145, Australia

Received 18 December 2003; received in revised form 22 June 2004; accepted 12 July 2004
Available online 27 August 2004

Abstract

This paper presents the results from using electroencephalographic (EEG) data to estimate the values of key neurophysiological parameters using a detailed biophysical model of brain activity. The model incorporates spatial and temporal aspects of cortical function including axonal transmission delays, synapto-dendritic rates, range-dependent connectivities, excitatory and inhibitory neural populations, and intrathalamic, intracortical, corticocortical and corticothalamic pathways. Parameter estimates were obtained by fitting the model's theoretical spectrum to EEG spectra from each of 100 healthy human subjects. Statistical analysis was used to infer significant parameter variations occurring between eyes-closed and eyes-open states, and a correlation matrix was used to investigate links between the parameter variations and traditional measures of quantitative EEG (qEEG). Accurate fits to all experimental spectra were observed, and both inter-subject and between-state variability were accounted for by the variance in the fitted biophysical parameters, which were in turn consistent with known independent experimental and theoretical estimates. These values thus provide physiological information regarding the state. transitions (eyes-closed vs. eyes-open) and phenomena including *cortical idling* and alpha *desynchronization*. The parameters are also consistent with traditional qEEG, but are more informative, since they provide links to underlying physiological processes. To our knowledge, this is the first study where a detailed biophysical model of the brain is used to estimate neurophysiological parameters underlying the transitions in a broad range (0.25–50 Hz) of EEG spectra obtained from a large set of human data.

Keywords: Cortex; Network; Physiology; Thalamocortical; Biophysics

1. Introduction

An integrated understanding of large-scale human brain function as a physiological and dynamical system has been difficult to achieve (Gordon, 2000), largely due to limitations on our ability to model and measure global brain functioning. Connectionist or neural-network modeling of neural populations has been important in the study of collective neural dynamics (e.g. Anderson, 1995; Elman, 1995; Gluck et al., 1992; Rumelhart, 1989; Rumelhart and McClelland, 1986). However, the connectionist approach has not been aimed at directly modeling neural activity; instead simulated measures have been in the form of abstract representations of environmental or cognitive states. Others have successfully modeled the tonic and phasic firing patterns of neuronal clusters and their effects upon distant neural populations (Lumer et al., 1997a, b; Suffczynski et al., 1999, 2001), and detailed models of mammalian thalamocortical systems have provided estimates of power spectra that are remarkably similar to those reported in the experimental literature (Lumer et al., 1997a, b). However, the level of empirical

*Corresponding author. The Brain Dynamics Centre, Westmead Hospital and University of Sydney, Westmead, New South Wales 2145, Australia. Tel.: +61-2-9351-5799; fax: 61-2-9351-7726.
E-mail address: drowe@physics.usyd.edu.au (D.L. Rowe).

0022-5193/$ - see front matter © 2004 Elsevier Ltd. All rights reserved.
doi:10.1016/j.jtbi.2004.07.004

description offered by these methods has not been commensurate with that needed to interpret direct measures of global cortical dynamics in humans. The electroencephalogram (EEG) is a more relevant goal for modeling global cortical dynamics, being a common clinical and experimental measure of the collective activity of localized regions of neocortical neurons (local field potentials) and the associated influence of neighboring and subcortical structures (Niedermeyer and Lopes da Silva, 1999).

We present here an approach to EEG interpretation that directly models the EEG using primary neurophysiological principles and structures; including axonal transmission delays, synapto-dendritic rates, separate excitatory and inhibitory neural populations, firing thresholds, nonlinearities, range-dependent connectivities, and cortical and subcortical networks. We thereby model both the spatial and temporal dynamics of cortical activity, and provide direct predictions of the EEG that can be used to infer global changes in human cortical dynamics in response to changes in arousal or cognition. This utilizes a two-dimensional continuum approach to model the neural activity in the cortex, with inputs from subcortical structures. The approach is based in part on earlier work by a number of authors, who have developed continuum based models and have made various comparisons with experimental findings (Freeman, 1975; Gill et al., 2002; Jirsa and Haken, 1996, 1997; Liley and Wright, 1994; Lopes da Silva et al., 1974; Nunez, 1974, 1995b; Rennie et al., 1999; Robinson et al., 1997, 1998, 2002; van Rotterdam et al., 1982; Wilson and Cowan, 1973; Wright and Liley, 1994, 1995).

The degree of neural structure incorporated has been chosen to capture key features of the EEG at multiple scales; including auditory event-related potentials (Rennie et al., 2002), 40 Hz intracortical gamma activity (Rennie et al., 2000), EEG waveforms and spectra in various seizure and arousal states (Robinson et al., 2002), correlation and coherence functions (Robinson, 2003), spatial spectra (O'Connor et al., 2002; O'Connor and Robinson, 2003), and scaling properties of EEG fluctuations (Robinson et al., 2004). In this study, the model is parameterized in terms of 10 physiologically relevant parameters. The number of parameters has been chosen so that parameters that do not impact on the variance of the data have been fixed, but close prediction of the important properties of the data can still been achieved. This has had the effect of maximizing the discriminatory power of the model parameters, as described in more detail in Sections 2.3 and 4.2 on Cerebral Connectivity and Parameters and Initialization, respectively.

In the current work we fit the model's theoretical EEG power spectrum to the eyes-closed and eyes-open power spectra from 100 human subjects to determine; (i) the feasibility of inferring physiological parameters by this means, (ii) the variance in the physiological parameter values for the 'normal' population, (iii) the parameter transitions occurring between these two states, (iv) the significance of the parameters in terms of physiological mechanisms contributing to the EEG, and (v) the relationship between the parameter transitions and traditional measures of quantitative EEG (qEEG). The model also provides a means for making direct predictions regarding parameter induced spectral changes, thus permitting the formulation of testable hypotheses. One must note that the model has a distributed structure, which means that the parameters function in an interdependent manner to collectivity influence the properties of the EEG, rather than representing localized 'pacemaker' type structures, as found in some other approaches (Destexhe et al., 1998b, 2002; Lehmann, 1971; Wang, 1999). Some of these approaches can have advantages for examining the neural dynamics of more localized populations including more detailed physiology and local phenomena such as the gamma rhythm and ion channel properties (Destexhe et al., 1998b, 2002; Freeman and Rogers, 2002) and nonlinear cortical phenomena (Freeman, 1987, 2003). However, they do not enable the examination of large-scale global dynamics that can permit probing of individual human EEG spectra, as in our approach. This, together with the models of more local neural dynamics, can provide a better understanding of neural activity across both microscopic and macroscopic scales.

To our knowledge, this is the first application where a whole-brain model has been used to successfully reproduce a broad range of human EEG spectra (0.25−49 Hz) from a large database, and explicitly determine underlying physiological parameters that are consistent with independent theoretical and experimental measures. Thus, the approach represents a significant technological advancement in the modeling of broad spectral human (or animal) EEG, which enables the localization of neural activity in specific primary pathways and neural populations according to transitions in cognitive or sensory activity, or state of arousal. Furthermore, the underlying model parameters may be used to accumulate a large database of physiologically significant values that can be used to understand normal and abnormal variants of human brain function in groups and individuals (Rowe et al., 2002b, 2004b).

In the following sections we summarize the basic EEG model and its use in fitting EEG spectral data to derive physiological parameters. In the Results section are plots and error values showing the high accuracy of the models fits, and statistical analyses comparing the various measures. In the Discussion the results are shown to be in good comparison with known experimental measures and theoretical estimates of physiology and traditional measures of qEEG. Also discussed, are

the role of the corticocortical and corticothalamic systems in the model, and possible mechanisms underlying the EEG phenomena, including sensory processing, cortical idling, alpha desynchronization, $1/f$ spectra and cortical stability.

2. Theory

2.1. Overview of the model

EEGs result from neural activity aggregated over scales much larger than individual neurons. This permits modeling the EEG using a continuum approximation that averages neural properties at a given point over a region of a few tenths of a millimeter. Fig. 1 is a schematic of the cortical connections, Fig. 2 shows the global structures including their large-scale connections. The schematics show that the model incorporates local inhibitory and excitatory connections resembling the short range stellate cells that contribute to intracortical connections. In addition, long range excitatory connections representing pyramidal cells form corticocortical and corticothalamic projections. The latter combine

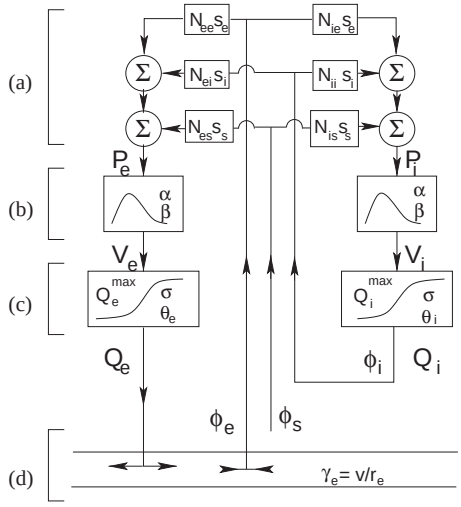

Fig. 1. Schematic representation of cortical connections. A single cortical unit is shown comprising a typical excitatory neuron on the left and an inhibitory neuron on the right. The four transformations that occur within neurons are represented by boxes: (a) a multiplication of afferent firing rates by synaptic numbers N_{ab} and strengths s_b, and spatial summation of fields $\phi_b\,(b = i, e, s)$ from inhibitory and excitatory subcortical (s, or thalamic relay) and cortical neurons (i, e); (b) temporal summation through convolution with a function parameterized by the rate constants α and β to produce a perturbation to the somatic membrane potential $V_a\,(a = e, i)$ at the cell body; (c) transformation of V_a by the sigmoidal function, characterized by threshold θ_a, width σ_a, and maximum firing rate $Q_a^{\max}$ and (d) propagation of excitatory impulses throughout the cortex as fields ϕ_a along axons according to a 2-D wave equation with damping rate γ_e. Those symbols appearing outside the boxes are functions of time, of which only ϕ_s is independent.

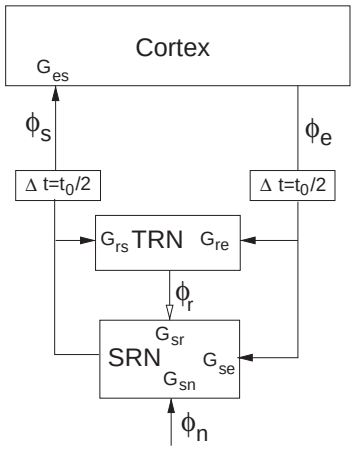

Fig. 2. Schematic showing primary pathways between the cortex, specific and secondary relay nuclei (SRN) and the thalamic reticular nucleus (TRN). The interconnections are shown with arrows; either solid (excitatory) or open (inhibitory). These provide two partially overlapping cortico-thalamocortical feedback pathways: one direct and excitatory between the cortex and SRN with total gain $G_{ese} = G_{es}G_{se}$; and one indirect and inhibitory pathway from cortex to TRN to SRN to cortex with total gain $G_{esre} = G_{es}G_{sr}G_{re}$. Intrathalamic feedback between the TRN and SRN is also possible, with gain $G_{srs} = G_{srGrs}$. Propagation between cortex and thalamus involves delays of $t_0/2$, and additional small delays are induced by each nucleus due to dendritic filtering. The firing rate in each pathway is $\phi_a, a = e, r, s$ and ϕ_N is an independent source of signals.

with thalamocortical relay projections to form corticothalamic loops, characterized by dense reciprocal connections between the cortex and relay cells in the dorsal thalamus. Inhibitory neurons of the thalamic reticular nucleus (TRN) in the thalamus also receive afferent projections from the cortex and form reciprocal connections with thalamocortical relay nuclei. These anatomical features are represented in the modeling of each neural population via the average firing activity or *pulse-densities* ϕ_a of the respective population—long-range excitatory pyramidal ϕ_e, short-range inhibitory and excitatory stellate ϕ_i (net inhibitory), thalamic relay ϕ_s, and thalamic reticular cells ϕ_r—together with their interconnections and external stimuli and driving input from ϕ_n. In the following sections we describe these populations in more detail, excluding the full mathematical analysis. This has been omitted for brevity, because it is explained fully elsewhere (Rennie et al., 1999, 2002; Robinson et al., 1997, 1998, 2001a, b, 2002, 2003a).

2.2. Neurophysiology

2.2.1. Neural activity

In the cortex, action potentials from various neurons, represented as neural fields ϕ_e, ϕ_i and ϕ_s, arrive at the dendritic tree (Fig. 1(a)). Their total effect is given by

$$P_a = v_{ae}\phi_e + v_{ai}\phi_i + v_{as}\phi_s. \quad (1)$$

The average response for inhibitory ($a = i$) and excitatory ($a = e$) cortical neurons is expressed as the sum of terms $v_{ab}\phi_b$ due to signals arising from neurons of type $b = e, i, s$. The parameter, $v_{ab} = N_{ab}s_b$ incorporates the average number of synapses N_{ab}, and the post-synaptic response s_b, to a unit input from neurons of type b.

We assume that the EEG ultimately reflects neural activity and given the large numbers of excitatory pyramidal cells ϕ_e in layers 3 and 5 of the cortex, we agree with others that these cells represent the principal source of the local field potentials (EEG) due to their large size and regular orientation (Niedermeyer and Lopes da Silva, 1999; Nunez, 1995b; Wright, 2000). Other cortical and subcortical structures ϕ_i and ϕ_s in the model, such as the thalamus are shown to exert significant effects upon these cells altering the frequency and strength of the EEG signal over long and short time scales (Rennie et al., 2002; Robinson et al., 1997, 2004). As has been shown previously, in the steady state model, when the system is driven by a constant, uniform mean stimulus level, ϕ_e can be used to calculate the EEG corresponding to the normal state (Robinson et al., 1997, 1998, 2001b).

2.2.2. Synaptic membrane potentials

The temporal spread and conduction delay within the dendritic tree of an individual neuron (Fig. 1(a)), leading to the membrane potential V_a at the cell-body (Fig. 1(b)), approximately obeys a convolution

$$V_a(\mathbf{r}, t) = \int_{-\infty}^{t} L(t - t')P_a(\mathbf{r}, t')\mathrm{d}t', \tag{2}$$

where $L(u)$ is the typical normalized dendritic impulse response function (Lopes da Silva et al., 1974). A suitable choice for $L(u)$ is

$$L(u) = \frac{\alpha\beta}{\beta - \alpha}(\mathrm{e}^{-\alpha u} - \mathrm{e}^{-\beta u}), \tag{3}$$

for $u > 0$, where dendritic rate constants β and α parameterize the rise and decay rate of the impulse response (Fig. 1(b)), respectively, and approximate the low pass response characteristics of the dendritic tree. The Fourier transform of $L(u)$ used in the final transfer function is

$$L(\omega) = (1 - \mathrm{i}\omega/\alpha)^{-1}(1 - \mathrm{i}\omega/\beta)^{-1}, \tag{4}$$

where $\omega = 2\pi f$ is the angular frequency and f is the frequency in Hz.

2.2.3. Neural impulse firing

The mean firing rate Q_a (or *pulse density*) of neurons occurring at the cell body (Fig. 1(c)) is assumed to vary according to a sigmoid function that relates firing rate to the average membrane potential V_a(2):

$$Q_a(\mathbf{r}, t) = \frac{Q_a^{\max}}{1 + \exp[-(\pi/\sqrt{3})\{V_a(\mathbf{r}, t) - \theta_a\}/\sigma_a]}, \tag{5}$$

where θ_a is the mean threshold activation for neurons of type a, σ_a is the standard deviation of this threshold for the neural population, and $Q_a^{\max}$ is the maximum attainable firing rate ($\sim 250\,\mathrm{s}^{-1}$). The value $\pi/\sqrt{3}$ has been carefully calculated in prior work, order that the standard deviation of the firing threshold of the neurons is σ rather than a multiple of σ. This is important in later analytical steps where the steady-state firing rate and the linear version of the model is calculated. The coordinate $\mathbf{r}$ refers to the position on the cortex, modeled as a two-dimensional sheet, which is justified by its relative thinness. Eq. (5) is a fair representation of the real nonlinear relationship between V_a and Q_a. However, if we treat the EEG signal as being due to small perturbations about a steady state, we can linearize the sigmoidal response by using the derivative $\rho_a = \mathrm{d}Q_a/\mathrm{d}V_a$ of the sigmoid at the steady state. This is commonly combined with the number and response strength of synapses to give the gains $G_{ab} = \rho_a N_{ab} s_b$ as shown in Fig. 2. These gains parameterize the differential number of neural pulses out per pulse in, and describe the effect of input perturbations from the various afferent neural fields ϕ_b on the firing rate Q_a of excitatory and inhibitory neurons ($a = i, e$) (Robinson et al., 1997, 2001b). The notation G_{ab} is such that the rightmost subscript refers to the source, and the leftmost refers to the destination (a standard convention in the physics of analogous systems).

2.2.4. Spreading activation

Action potentials propagate away from the cell body along a branching axon forming the neural fields or pulse densities ϕ_a (Fig. 1(d)). On average, the potentials propagate at a velocity $v_a \sim 10\,\mathrm{ms}^{-1}$ (Bullier and Henry, 1979; Dinse and Kruger, 1994; Nunez, 2002), with decreasing effect at greater distances due to decreasing terminal density. Propagation can be approximated by a damped wave equation representing the average spread of the electrical wave generated from a population of neurons

$$D_a\phi_a(\mathbf{r}, t) = Q_a(\mathbf{r}, t), \tag{6}$$

$$D_a = \frac{1}{\gamma_a^2}\left[\frac{\partial^2}{\partial t^2} + 2\gamma_a\frac{\partial}{\partial t} + \gamma_a^2 - v^2\nabla^2\right], \tag{7}$$

where $\gamma_a = v_a/r_a$ is the damping rate and r_a is the characteristic range of axons of type a (Jirsa and Haken, 1996; Robinson et al., 1997).

The connectivities between various neural populations, and the associated physiological parameters shown in Table 1 are described in the following sections. Many values for the parameters have been inferred from

Table 1
Physiological estimates of parameters of the model as discussed in references (Braitenberg and Schüz, 1991; Niedermeyer and Lopes da Silva, 1999; Nunez, 1995b; Rall, 1967; Rennie et al., 2000; Robinson et al., 1997; Wilson and Cowan, 1973)

Quantity	Range	Nominal	Unit
$\sigma_{e,I}$	3–8	3.3	mV
$\theta_{e,I}$	10–25	15	mV
α	35–150	40	s^{-1}
β/α	1–8	4.0	—
r_e	60–100	80	mm
r_i, r_r, r_s	~0.1	—	mm
v_a	5–10	8	$m\,s^{-1}$
t_0	60–100	84	ms
K_0	10–50	30	m^{-1}
v_{ee}, v_{es}, v_{se}	0.05–10	1.2	mV s
$-v_{ei}$	0.05–10	1.8	mV s
v_{re}	0.05–10	0.4	mV s
v_{rs}	0.05–10	0.2	mV s
$-v_{sr}$	0.05–10	0.8	mV s
$v_{sn}\phi_n$	0.05–10	1.0	mV s
γ_e	50–200	130	s^{-1}
$\gamma_i, \gamma_r, \gamma_s$	$\sim 10^4$	—	s^{-1}
Q_a	100–1000	250	s^{-1}
ρ_a	1000–6000	—	$V^{-1}\,s^{-1}$
G_{ee}	1–20	6	—
$-G_{ei}$	1–20	7	—
$-G_{srs}$	0.01–2.5	0.4	—
$-G_{esre}$	0.5–10	3	—
G_{ese}	0.1–10	5	—

Limits are approximate.

physiology while others are much more loosely constrained a priori, but are obtained more precisely in this study.

2.3. Cerebral connectivity

2.3.1. Local and intracortical connections

The axonal range of stellate cells ($r_i \sim 0.1$ mm) is significantly shorter than the axons of pyramidal cells ($r_e \sim 80$ mm) and significantly smaller than the minimum scale of EEGs (10−50 mm for scalp recordings). This permits us to assume that for local neural populations axonal lengths and delays can be neglected. Given this assumption the local inhibitory and excitatory field ϕ_i in Eq. (1) can be replaced by Q_i, and smallness of r_i also lets us set $\gamma_i \approx$ infinity (Robinson et al., 1997, 2001b).

2.3.2. Corticocortical and corticothalamic connections

The axons from pyramidal cells form dense synaptic connections with the local neurons including stellate cells and other pyramidal cells, but also form long range corticocortical and subcortical connections, which decrease in synaptic density as axonal range increases. This property of the pyramidal neuron is reflected in the equation for axonal propagation in Eq. (7), which implies that terminal density decreases at an approximately exponential rate at long ranges (Robinson et al., 1997, 2001b) in accord with experimental work (Braitenberg and Schüz, 1991).

The signals ϕ_s returning to the cortex from subcortical structures are a mixture of sensory signals and activity from corticothalamic pathways. The neurophysiology of the subcortical neurons remains the same as previously explained. However, the additional nuclei in the pathways and the associated axonal projections induce further delays in signal propagation that contribute to the resonant properties of the system. Fig. 2 shows the primary corticothalamic and intrathalamic pathways used in the model, plus the inherent transmission delays $t_0/2 \sim 0.04$ s. In each direction the various gains G_{ab}, with additional type b neurons—s, r, and n referring to specific relay nuclei (SRN), the TRN, and external signals, respectively, with ϕ_n including both brain stem reticular activation and stimuli.

The corticothalamic feedback path is comprised of neural activity generated by excitatory corticothalamic efferents ϕ_e that synapse with relay nuclei (with gain G_{se}) and then return to the cortex via thalamocortical afferents (with gain G_{es}). Activation of the pathway involving G_{es}, G_{se}, and dendritic filtering induces a signal delay time of approximately 0.1 s, resulting in a strong alpha resonance when the loop gain is adequate. The total gain $G_{ese} = G_{es}G_{se}$ is positive since both G_{es} and G_{se} are gains of excitatory neurons. There is also a negative feedback pathway involving corticothalamic signals that pass through the inhibitory TRN (with gain G_{re}), then the relay nuclei (G_{sr}), before returning to the cortex via thalamocortical afferents ϕ_s (G_{es}), with overall gain $G_{esre} = G_{es}G_{sr}G_{re}$. The inhibitory reticular neurons means that G_{sr} and the total loop gain G_{esre} are negative. At high values, this loop gain can lead to strong resonance within the θ band due to the inversion of the positive corticothalamic feedback signal and the resultant modulation of ϕ_e in the cortex. The third and final loop illustrated in Fig. 2 is the intrathalamic loop with total inhibitory gain $G_{srs} = G_{rs}G_{sr}$. This pathway has a very short delay time such that adequate gain may lead to strong resonance corresponding to the spindle frequency ~12–15 Hz (Robinson et al., 2001b, 2002, 2003a).

In the Fourier domain, ϕ_s can be written as

$$\phi_s = T\phi_n + S\phi_e, \tag{8}$$

where

$$T = \frac{LG_{sn}e^{i\omega t_0/2}}{1 - LG_{sr}LG_{rs}} \tag{9}$$

and

$$S = \frac{(LG_{se} + LG_{sr}LG_{re})e^{i\omega t_0/2}}{1 - LG_{sr}LG_{rs}}, \tag{10}$$

where T is the thalamic transfer function and S is the corticothalamic transfer function in Fourier space (Rennie et al., 2002; Robinson et al., 2001b). L is the dendritic filtering given in Eq. (4) and t_0 is the delay in the corticothalamic loop. As with the *local* intracortical connections described above, for thalamic nuclei, given their local proximity, we can make the local approximation such that $\phi_r = Q_r$, $\phi_s = Q_s$, and $\gamma_r = \gamma_s \approx$ infinity. The driving signal ϕ_n is approximated as white noise in space and time, as in our previous work (Robinson et al., 2001b, 2002, 2003a).

2.3.3. Cortical boundaries

In previous studies using the continuum approach the basic physiological structure utilized a two-dimensional unbounded cortex (Robinson et al., 1997, 1998, 2001a, b). It was shown that the typical damping rate of the cortex was sufficiently large that boundary conditions could be ignored for many purposes since these components did not result in substantial changes to the EEG (Robinson et al., 1997, 2001a, 2003a). However, in the present work, the inclusion of boundary conditions or modal effects was found to improve fits to EEG data displaying steep $1/f$ spectra and sharp alpha peaks, consistent with the modal analysis of Robinson et al. (2001a).

2.4. Theoretical spectra

2.4.1. EEG spectra

By linearizing Eq. (5) and combining the Fourier domain forms of the remaining equations (Robinson et al., 2001b) one obtains the following expression for the spectral power density:

$$P_{\rm EEG}(\omega) = P_0 \left| \frac{L(\omega)T/G_{sn}}{1 - G_{ie}L(\omega)} \right|^2 \frac{(2\pi)^2}{l_x l_y} \times \sum_{m,n=-\infty}^{\infty} \frac{{\rm e}^{-k_{m,n}^2/k_0^2}}{|k_{m,n}^2 r_e^2 + q^2(\omega) r_e^2|^2}, \quad (11)$$

where

$$q^2(\omega) r_e^2 = \left(1 - \frac{{\rm i}\omega}{\gamma_e}\right)^2 - \frac{G_{ee}L(\omega) + G_{es}L(\omega)S}{1 - G_{ei}L(\omega)}, \quad (12)$$

$$P_0 = \frac{\pi |\phi_n|^2}{r_e^2} G_{es} G_{sn}, \quad (13)$$

and the discrete wave numbers $k_{m,n}$ are defined by

$$k_{m,n}^2 r_e^2 = (2\pi m r_e/l_x)^2 + (2\pi n r_e/l_y)^2. \quad (14)$$

Subscripts m and n are mode numbers (relating to the cortical boundaries), which can be restricted to values $< f_{max}/2$ in magnitude without significant loss of accuracy, given f_{max} is the maximum frequency of interest (Robinson et al., 2001a). In this study f_{max} was = 49 Hz. The parameter, P_0 is adjusted by the fitting routine according to the overall amplitude of the experimental power spectrum and combines several quantities that affect the overall scale of the theoretical power spectrum, without affecting its shape. The factor ${\rm e}^{-k_{m,n}^2/k_0^2}$ is introduced in Eq. (11) to approximate the filtering of high-spatial frequencies k due to volume conduction by the cerebrospinal fluid, skull and scalp (Rennie et al., 2002; Robinson et al., 2001a).

2.4.2. EMG spectra

The tonic or burst firing of pericranial muscles known as electromyogram (EMG) can cause apparent power enhancements in the EEG spectra above approximately 25 Hz. This is consistent with our observations (and others) of enhanced spectral power at high frequencies (>25 Hz) during conditions of jaw clenching, frowning and other facial movements (Shwedyk et al., 1977; van Boxtel et al., 1983; van Boxtel, 2001). If not accounted for, these changes can affect the interpretation of spectra in terms of physiology. To compensate for EMG artefact we used a theoretical model of the resulting spectral contribution, that has been empirically verified, and which was used to determine the optimum bandwidth for the measurement of pericranial EMG (Shwedyk et al., 1977; van Boxtel et al., 1983; van Boxtel, 2001).

The form of the EMG model spectrum used here is

$$P_{\rm EMG}(f) = \frac{A(f/f_c)^2}{[1 + (f/f_c)^2]^{1+\delta/2}}, \quad (15)$$

where f_c refers to low frequency cut-off, δ the high frequency asymptotic power law index (with $P(f) \propto f^{-\delta}$ at large f), and A the power normalization factor. The frequency of the EMG spectral peak in Eq. (15) is

$$f_{pk} = \sqrt{\frac{2}{\delta}} f_c. \quad (16)$$

Note the frequency response property of Eq. (15) is different to that of the dendritic rate parameter α, which affects a similar frequency range. Therefore, the EMG correction algorithm is not expected to have a strong influence upon the estimation of α (see Section 5.2: EMG parameter).

3. Subjects EEG data and processing

3.1. EEG data

EEG recordings of healthy adult subjects from the general community were obtained with the appropriate ethical clearances and informed consent, and screened for any history of substance abuse or dependence, epilepsy, other neurological disorders,

mental retardation or head injury (Bahramali et al., 1997, 1998, 1999). Subjects were 49 females and 51 males with a mean age of 44 years ($SD = 16$ years) and 45 years ($SD = 15$ years), respectively. The subjects were awake and non-drowsy throughout the recordings. The EEGs were acquired as part of a battery of electrophysiological tests. Only the EEG measures at the central site Cz from the eyes-closed and eyes-open states were used in this study, with more complex multi-site analyses being left for later work. During the eyes-open recording subjects were instructed to fixate on a central fixation point displayed on a monitor directly ahead.

An electrode cap using the international 10–20 system of scalp sites was used to acquire the EEG data. EEGs were recorded at a 250 Hz sampling rate and an A/D precision of 0.42 uV through a SynAmps™ amplifier using a linked ear-lobe reference and a low-pass third-order Butterworth filter with –6 dB point at 50 Hz. Eye movements in particular, can affect the low frequency component of the EEG spectra and therefore the cortical gains. Such ocular (horizontal, vertical, and blink) movements were corrected offline according to the method of Gratton et al. (1983). This is a commonly used method in EEG studies and is considered sufficient for our purposes. More discussion of the possible effects of eye movements on EEG data is provided in references (Croft and Barry, 2000; Joyce et al., 2004).

3.2. EEG spectral data

For each EEG recording the average experimental power spectrum P_{exp} from 0.25 to 50 Hz (210 data points) was calculated for 27 successive 4 s epochs using a Fast-Fourier transform analysis. The standard deviation σ of the experimental spectrum at each frequency was also calculated over the 27 epochs.

3.3. qEEG values

In order to compare with traditional phenomenological qEEG, *relative* (i.e. fractional) powers for each subject's experimental spectrum were calculated for the following frequency bands; slow wave (0.25–1.0 Hz), delta (1.25–3 Hz), theta (3.25–7 Hz), alpha (7.25–13 Hz), beta–1 (13.25–20 Hz), beta–2 (20.25–25 Hz), beta–3 (25.25–30 Hz), and gamma (30.25–48 Hz) frequency bands. The ranges were selected based on a 0.25 Hz frequency resolution and were approximated from typical psychophysiological studies examining qEEG in eyes-closed states (Lazzaro et al., 1998; Martinovic et al., 1998; e.g. Omori et al., 1995). The resultant qEEG band values were calculated in *relative* power by dividing the band power by the total spectral power, and denoted as $P_{sw}, P_{\delta}, P_{\theta}, P_{\alpha}, P_{\beta 1}, P_{\beta 2}, P_{\beta 3}$, and P_{γ}, in that order.

4. Data fitting and parameter initialization

4.1. Data fitting

In model fitting, we form the sum of the EEG spectrum in Eq. (11) $P_{\mathrm{EEG}}(f)$ and an EMG component in Eq. (15) $P_{\mathrm{EMG}}(f)$, and fit this to the experimental power spectrum $P_{exp}(f)$ at site Cz, such that the estimated power spectrum is given by

$$P_{\mathrm{est}}(f) = P_{\mathrm{EEG}}(f) + P_{\mathrm{EMG}}(f). \tag{17}$$

To minimize noise in $P_{exp}(f)$ smoothing of the log-transformed spectrum at Cz was performed by convolution with a Gaussian having a specified $SD = 1$ Hz. The range of the Gaussian was normally ± 3 SD, but this range was symmetrically reduced when smoothing the low and high frequency extremes since the power spectrum is defined only over a finite range. The chi-squared error χ^2 between P_{exp} and P_{est} is reduced by parameter optimization using the Levenberg-Marquardt method (Press et al., 1992), in which χ^2 is calculated as follows:

$$\chi^2 = \sum_{I=1}^{N} \frac{[\log_e(P_{exp}(f_i)) - \log_e(P_{est}(f_i))]^2}{\sigma_i^2}, \tag{18}$$

where each difference is weighted by the inverse of the corresponding variance $1/\sigma_i^2$. Parameter adjustments continue until $\chi^2 < 50$ is achieved, to ensure a close fit. If $\chi^2 < 50$ is attained, then iteration ceases on the first occasion that the change in χ^2 satisfies $\Delta\chi^2 < 0.01$. Further iterations beyond $\Delta\chi^2 < 0.01$ are generally wasteful since changes in $\chi^2 \ll 1$ are never statistically meaningful, and it is not uncommon to find parameters drifting near the minimums of a very "flat" valley in the χ^2 'landscape' (Press et al., 1992).

An additional weighting is applied to compensate for the many data points for high frequency features (e.g. β), compared with far fewer for low frequency features (e.g. Δ). For example, there might be 10 points in the range 1–10 Hz, but 90 points in the range 11–100 Hz (the next decade). Accordingly, calculation of χ^2 is weighted by an additional factor $1/f$, thereby maintaining fits based on spectral detail per decade rather than the number of data points. We also decrease the weighting to zero at 50 Hz to suppress the influence of mains voltage interference.

The final requirement in data fitting is the specification of the fixed and initial free parameter values, and their limits listed in Table 2. A description of their selection and properties follows.

4.2. Parameters and initialization

Examination of the theoretical EEG spectra in Eq. (11) reveals the 14 parameters for the model listed

Table 2
Initial and *fixed parameter values for the EEG and EMG theoretical model spectrum, obtained from previous experimental work and references

Model	Parameter	Description	Limits	Initial Value
EEG Model	γ_e	Cortical damping (v_e/r_e)	40–400	$130\,s^{-1}$
	α	Dendritic decay rate	10–200	$75\,s^{-1}$
	β	Dendritic rise rate	—	3.8α*
	t_0	Conduction delay through thalamic nuclei and projections.	0.06–0.13	0.084 s
	G_{ee}	Excitatory gain–pyramidal cells	0–50	5.4
	G_{ei}	Local intracortical gain–stellate cells	−35–1	7.0
	G_{ese}	Corticothalamocortical gain via SRN	0–50	5.6
	G_{esre}	Corticothalamocortical gain via TRN	−30–0	−2.8
	G_{srs}	Intrathalamic gain	−15–0.5	−0.6
	k_0r_e	Volume conduction filter parameter	—	3.0*
	l_x, l_y	Linear dimensions of cortex	—	0.5 m*
	r_e	Characteristic pyramidal axon length	—	0.08 m*
	P_0	Overall power normalization (Eq. (13))	—	Calculated
EMG	A	Power normalization	0–99	$0.5\,\mu V^2\,Hz^{-1}$
	f_{pk}	Spectra peak frequency	—	40 Hz*
	δ	Asymptotic slope	—	2*

All values are consistent with independent sources and physiological measures (Nunez, 1995b; Rall, 1967; Rennie et al., 2002; Robinson et al., 1997, 2001b; Shwedyk et al., 1977; Stulen and DeLuca, 1981; van Boxtel, 2001). Limits refer to the restricted ranges in which parameters are free to vary.

in Table 2. Variations of some of these within any physiologically reasonable range have little effect on the spectrum (Rennie et al., 2002; Robinson et al., 2001b). Explorations of variants of the model with significantly more parameters have also shown that the use of too many additional parameters leads to an increase in fit error and inability to obtain robust estimates of the parameters (Rowe et al., 2002a, b). Here, we have obtained a balance that optimizes the number of parameters and incorporates a degree of neural structure that is sufficient to generate accurate and reliable predictions of spectral changes in the EEG. We have also found that during the fitting procedure, in a small number of cases, parameter values may drift within relatively wide valleys that reflect broad local minimum, before converging to a global minimum that is within physiological limits. Therefore, to assist the fitting procedure, broad parameter limits are set (Table 2), such that beyond these limits, χ^2 is modified by a multiplicative factor that increases quadratically when the physiologically realistic range for parameter is exceeded. This allows the fitting routine to adjust parameter back to within the parameter limits until a physiologically realistic local minimum is found. These limits thereby improve the convergence of the model parameters in those cases where high uncertainty exists in the data, typically in noisy and/or featureless spectra.

Cortical dimensions l_x and l_y (0.5 m), cranial filtering parameter k_0r_e, and axonal range r_e can be fixed at the values estimated from references. An exception is $\beta/\alpha = 3.8$, which was obtained empirically in earlier studies by fitting the theoretical spectrum in Eq. (17) to the 100 normal eyes-closed data set, and allowing β/α to vary within the limits $1<\beta/\alpha<20$ (Rowe et al., 2001, 2002a, b). A median of 3.8 was obtained and found to be consistent with ranges obtained from independent experimental measures and theoretical estimates (Kim et al., 1997; Lopes da Silva et al., 1974; Lumer et al., 1997a, b; Suffczynski et al., 2001; van Rotterdam et al., 1982).

The average parameter values calculated from the eyes-closed condition in the earlier studies also provided the initial values for the free parameters listed in Table 2. With the exception of fixed values, these are used for convenience, given multiple initial values set during the fitting procedure have been found to yield the same spectral fit and end parameter values to within uncertainties (Rowe et al., 2002a, b). The overall power normalization parameter P_0 (Table 2) is calculated from the experimental data and is related to the model parameters $G_{es}G_{sn}$, ϕ_n and r_e as in Eq. (13). It is adjusted during fitting according to the overall power of the experimental spectrum and permits the experimental and theoretical spectra to have equal total powers during fitting.

In the equation for EMG Eq. (15), values for $f_c = f_{pk}$ and δ were fixed at their values listed in Table 2. These were estimated from the results of Van Boxtel (2001) and are consistent with data from Stulen and Deluca (1981). The initial value of the EMG power normalization factor A was estimated *post hoc* in earlier experimental development by carrying out fits to experimental data using initial values ranging from 0.1–1.0 $\mu V^2/Hz$. The value of $0.5\,\mu V^2/Hz$ was found to be the optimal starting value for parameter convergence in this data set.

4.3. Theoretical (predicted) spectrum and parameter sensitivities

The sensitivities of the theoretical spectrum to key parameters are illustrated in Fig. 3, consistent with previous work by Robinson et al. (2001b) and Rennie et al. (2002). The sensitivity plots can be used to predict spectral changes as a result of parameter variations and thereby formulate testable hypotheses (e.g. that certain changes in spectral shape will be associated with changes in particular parameters) and infer associated physiological changes: (a) An increase in cortical damping γ_e results in more rapid dissipation of pulses outgoing from each location, but simultaneously restricts them to a smaller area (if the axonal velocity is unchanged). This leads to a higher power overall, particularly at the alpha

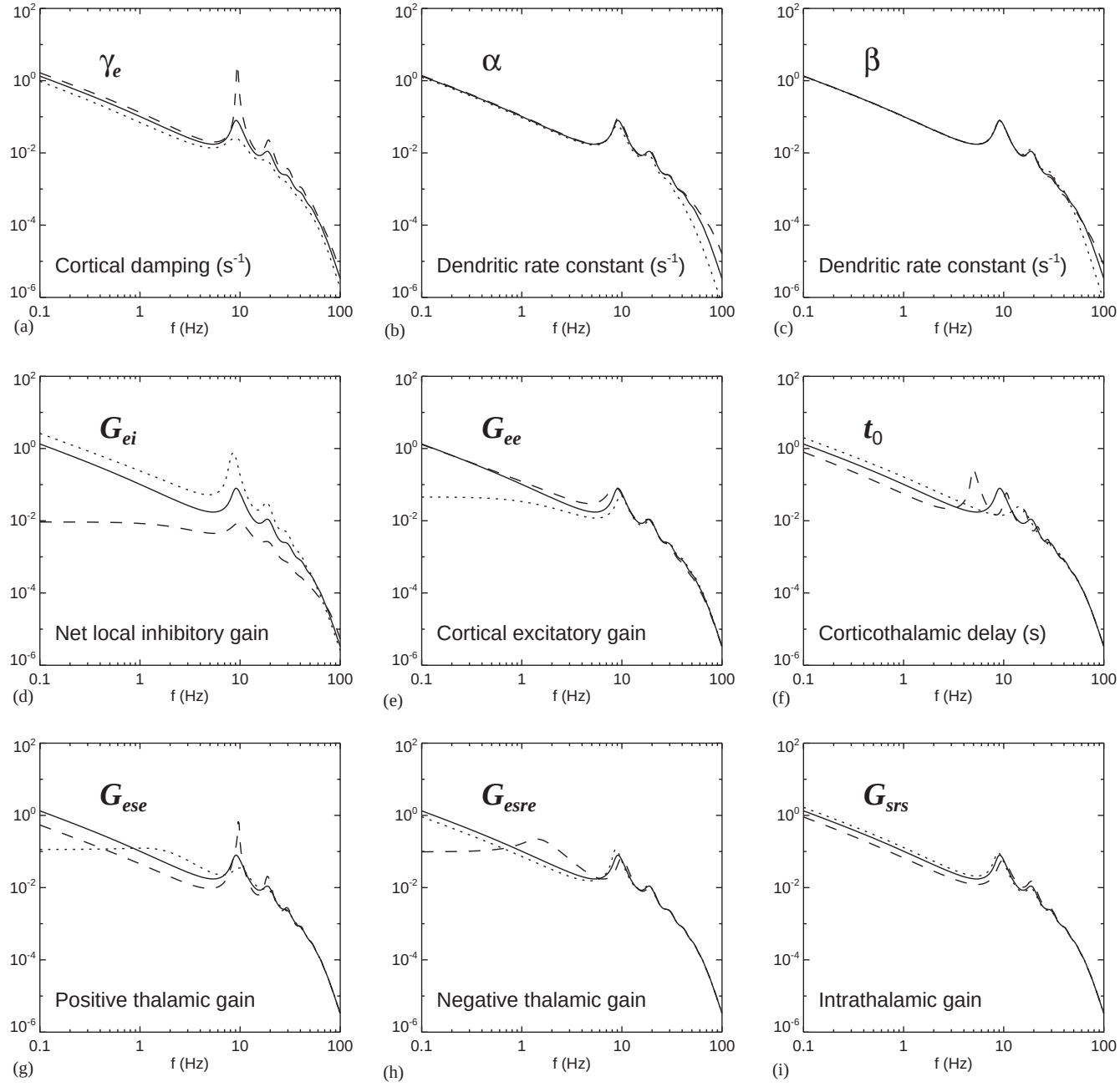

Fig. 3. Parameter sensitivities and their independent effects on spectral detail are illustrated for each parameter for 3 values of increasing magnitude, … × 0.5, — × 1.0,- - - × 2.0. Parameter values are arbitrary and illustrative of the trends in spectral change as a result of the parameter variations. In (a), change in cortical damping, …70, — 140 ,- - -280, (b) dendritic rise rate parameter α, …38, — 75 ,- - -150, (c) dendritic decay rate parameter β, …150, — 300,- - -600, (d) net local inhibitory neural $|G_{ei}|$ …2.8, — 5.5,- - -11.0, (e) cortical excitatory gain …3.0, — 6.0 ,- - -12.0, (f) corticothalamic delay …0.04, — 0.08,- - -0.16, (g) positive thalamic gain …3.2, — 6.3,- - -12.6, (h) negative thalamic gain $|G_{esre}|$ …1.6, — 3.3,- - - 6.6, and (i) intrathalamic gain $|G_{srs}|$ …0.25, — 0.5 ,- - -1.0.

and beta resonance due to corticothalamic feedback (Robinson et al. 2001b). (b and c) The increase in the dendritic rate parameters α and β reduces the degree of low-pass filtering in neurons, and so enhances the high frequency component (>20 Hz) of the spectra. (d) The change in net local neural gain G_{ei} has a strong effect on the lower frequency $1/f$ component (0−7 Hz) of the spectrum as well as the alpha and beta resonance. Increased ($|G_{ei}|$, more negative) values lead to reduced power across the entire frequency range, particularly the $1/f$ range of the spectra. (e) Changes in cortical excitatory gain G_{ee} have the opposite effect, with increases (more positive) leading to enhancement of the $1/f$ low frequency component of the spectrum. (f) Corticothalamic delay t_0 affects the resonant frequencies of the EEG, with shorter delays shifting the resonant peaks such as alpha and beta peaks to higher frequencies. (g) The positive thalamic feedback loop G_{ese} has a particularly strong affect on the alpha and beta resonances, with increased G_{ese} leading to stronger resonances. As $G_{ese} \to 0$ (decreases), this increases the relative proportion of the other (negative) corticothalamic feedback loop G_{esre}, and so enhances delta (~1 Hz) and theta (3–7 Hz) frequencies, but decreases alpha resonances, as shown in (h). (i) Increases in the negative intrathalamic feedback $|G_{srs}|$ will uniformly attenuate the low frequency $1/f$ component of the spectra. Note, that although the above parameters are treated in this figure as if independent, they may in practice covary in experimental data.

5. Results

5.1. Fits to experimental data

5.1.1. Goodness of fit

A sample of fits to six typical subjects' eyes-closed and eyes-open EEG recordings with variability in alpha and beta peaks is illustrated in Fig. 4. Close agreement is seen between each fitted theoretical spectrum and the corresponding experimental spectrum across the various alpha–beta peak combinations, and the corresponding eyes-open state. The χ^2 error ('goodness of fit') produced values ranging from 2.9 to 49.8, with a mean of 30.7 ($SD = 13.7$) in the eyes-closed condition, and 26.8 ($SD = 14.5$) in the eyes-open condition. Using the χ^2 test for these values, there was no evidence to suggest a significant difference between the theoretical and experimental spectra [$p > 0.995$, *degrees of freedom* = 99].

5.1.2. EEG model parameters

The fits to the experimental spectrum yield nine independently fitted physiological parameters (Table 2) for each subject's eyes-closed and eyes-open states. Of these, the overall EEG power normalization P_0

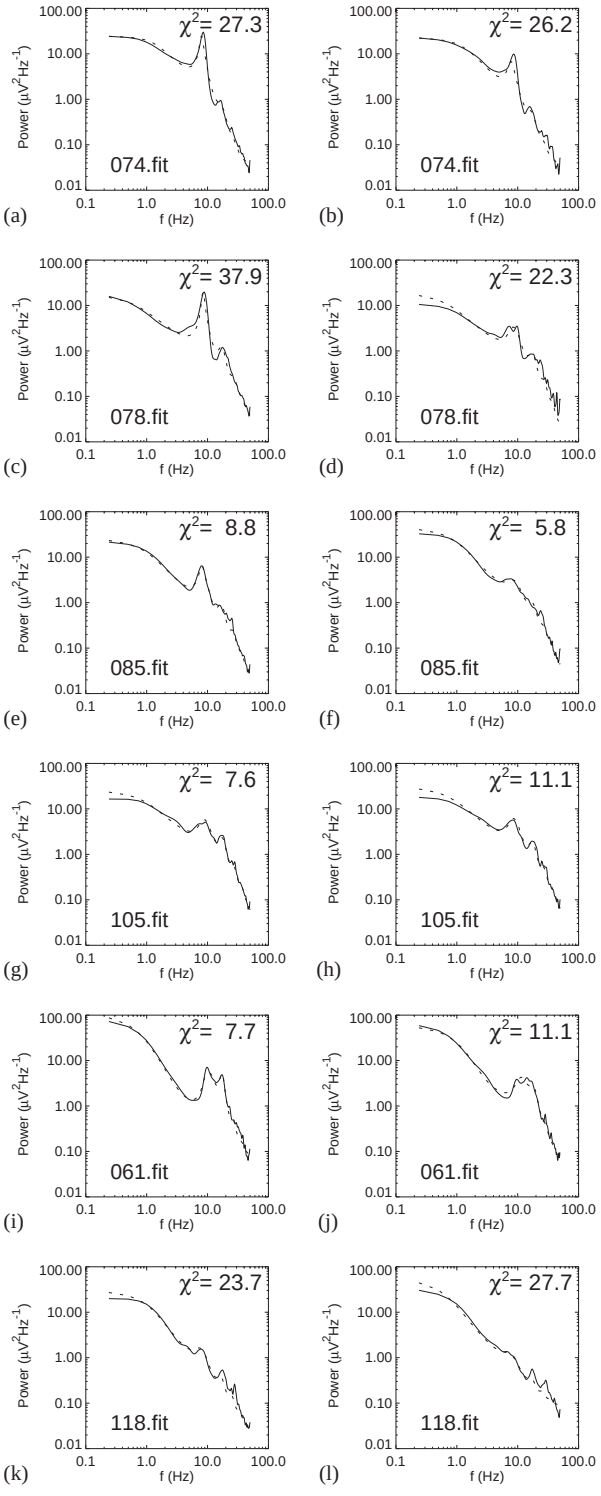

Fig. 4. Sample of model fits for 6 subjects varying in χ^2 error. In column (i), frames from top to bottom vary qualitatively in the relative and absolute strengths of the alpha and beta peaks in the eyes-closed state, with the corresponding eyes-open state on the right. Each frame compares a subject's experimental spectra (−) with their modeled spectra (…), and lists the subject's ID number and corresponding χ^2 value reflecting goodness of fit. Figure (a) shows strong alpha peak with very small beta peak, (c) strong alpha peak with beta peak, (e) wide alpha peak with very small beta peak, (g) small alpha and beta peak, (i) large alpha and beta peak, and (k) very small alpha and beta peak.

(Eq. (13)) is proportional to unknown factors relating power to experimental spectra such as net attenuation through the skull and scalp. Eq. (13) also shows P_0 is also a factor of ϕ_n, and $G_{es}G_{sn}$, referring to brain stem and stimulus activation, which is transferred to the cortex via TC projections G_{es} (Fig. 2). As shown in Table 3, there was a relatively small decrease in P_0 in the eyes-open condition compared with eyes-closed, suggesting a reduction in one of these parameters, most likely G_{es}, given the significant decrease in G_{ese} in the eyes-closed condition (Table 3). Frequency histograms are shown in Fig. 5 for the remaining eight physiological parameters measured for the eyes-closed and eyes-open states. The parameter values fall within the expected physiological ranges, with the exception of outlying parameter values in five subjects, which were found to converge upon the parameter limit boundaries (Table 2). In the eyes-closed condition, outliers occurred for γ_e in three subjects, for α in one subject and G_{ee} in one subject. One of these same subjects and an additional subject also had an outlying value for α in the eyes-open condition. These outlying values possibly occurred due to noise and/or featureless spectra. Note, with the removal of these outliers and a reanalysis of the data did not alter the statistically significant results that follow below. Further observations are that cortical damping γ_e and excitatory gain G_{ee} show relatively tight normal distributions in the eyes-closed condition but less so in the eyes-open condition, and that the corticothalamocortical delay parameter t_0 shows almost identical normal distributions across states. Both γ_e and t_0 are expected to be relatively constant across states given that they largely reflect constants of physiology and/or development. The remaining physiological parameters show relatively good normal distributions.

Table 3
Comparison of mean Model parameter values and qEEG values for relaxed eyes-closed vs. eyes-open conditions, shown with standard error of the mean, and t statistic. Bolding, * denotes t values reaching significance at $p<.005$, obtained using a paired-samples t-test.

Parameter	Mean	Std. Error (SE)	t[1, 99]
EEG Model Parameters			
γ_e (ec)	140	7	**4.05***
	116	4	
α (ec)	75	3	**5.69***
(eo)	93	4	
$t0$ (ec)	0.084	0.001	1.55
(eo)	0.085	0.001	
G_{ei} (ec)	−7.5	0.2	2.11
(eo)	−8.1	0.3	
G_{ee} (ec)	5.8	0.2	**3.18***
(eo)	6.8	0.3	
G_{ese} (ec)	5.4	0.2	**6.73***
(eo)	4.2	0.2	
G_{esre} (ec)	−3.3	0.1	1.22
(eo)	−3.1	0.1	
G_{srs} (ec)	−0.50	0.05	**3.22***
(eo)	−0.37	0.05	
P_0 (ec)	2.49	0.03	**3.49***
(eo)	2.40	0.02	
qEEG (relative power)			
P_{sw} (ec)	0.12	0.02	2.52
(eo)	0.16	0.02	
P_δ (ec)	0.175	0.007	**9.80***
(eo)	0.190	0.006	
P_θ (ec)	0.138	0.005	**3.03***
(eo)	0.173	0.005	
P_α (ec)	0.139	0.005	**9.75***
(eo)	0.150	0.005	
$P_{\beta 1}$ (ec)	0.30	0.01	2.40
(eo)	0.21	0.01	
$P_{\beta 2}$ (ec)	0.092	0.005	**4.45***
(eo)	0.097	0.005	
$P_{\beta 3}$ (ec)	0.040	0.003	**6.41***
(eo)	0.047	0.003	
P_γ (ec)	0.022	0.002	**5.62***
(eo)	0.027	0.002	

5.1.3. EMG parameter

The effect of the EMG correction in Eq. (15) on the theoretical EEG spectra in Eq. (11) for the eyes-closed condition is illustrated in Fig. 6 for a typical subject where the EMG power normalization A approximates the group mean. This illustrates that the overall shape of the total spectrum is unaffected by EMG. There is only a small enhancement relative to the 'pure' EEG spectrum at high frequencies (>25 Hz). As is expected in the case of EMG artefact due to its high frequency characteristics (van Boxtel, 2001). A strong skewness in the distribution of this parameter is also illustrated in Fig. 5, showing a large proportion of subjects displayed relatively minimal levels of EMG.

5.2. Parameter differences between eyes-closed and eyes-open

5.2.1. EEG model parameters

The mean values of the physiological parameters in each of the measured states are listed in Table 3. These values were consistent with preliminary estimates used in previous work (Robinson et al., 2002). The differences in the mean values between states were tested for significance using a paired-samples t-test (Table 3). To control for false positives due to repeated comparisons, only significance levels of $p<0.005$ are accepted as significant in this study. Significant differences were found for $\alpha, \gamma_e, G_{ee}, G_{ese}$, and G_{srs}. In the eyes-open relative to the eyes-closed state: cortical damping γ_e was weaker, gain parameters G_{ese} and G_{srs} were smaller, and G_{ee} and α was higher.

5.2.2. EMG parameter

The mean value for the EMG parameter A was calculated as $0.124\,\mu V^2/Hz$ ($SD=0.173$) in the eyes-closed condition and $0.157\,\mu V^2/Hz$ ($SD=0.196$) in the eyes-open condition. There was reason to suggest the

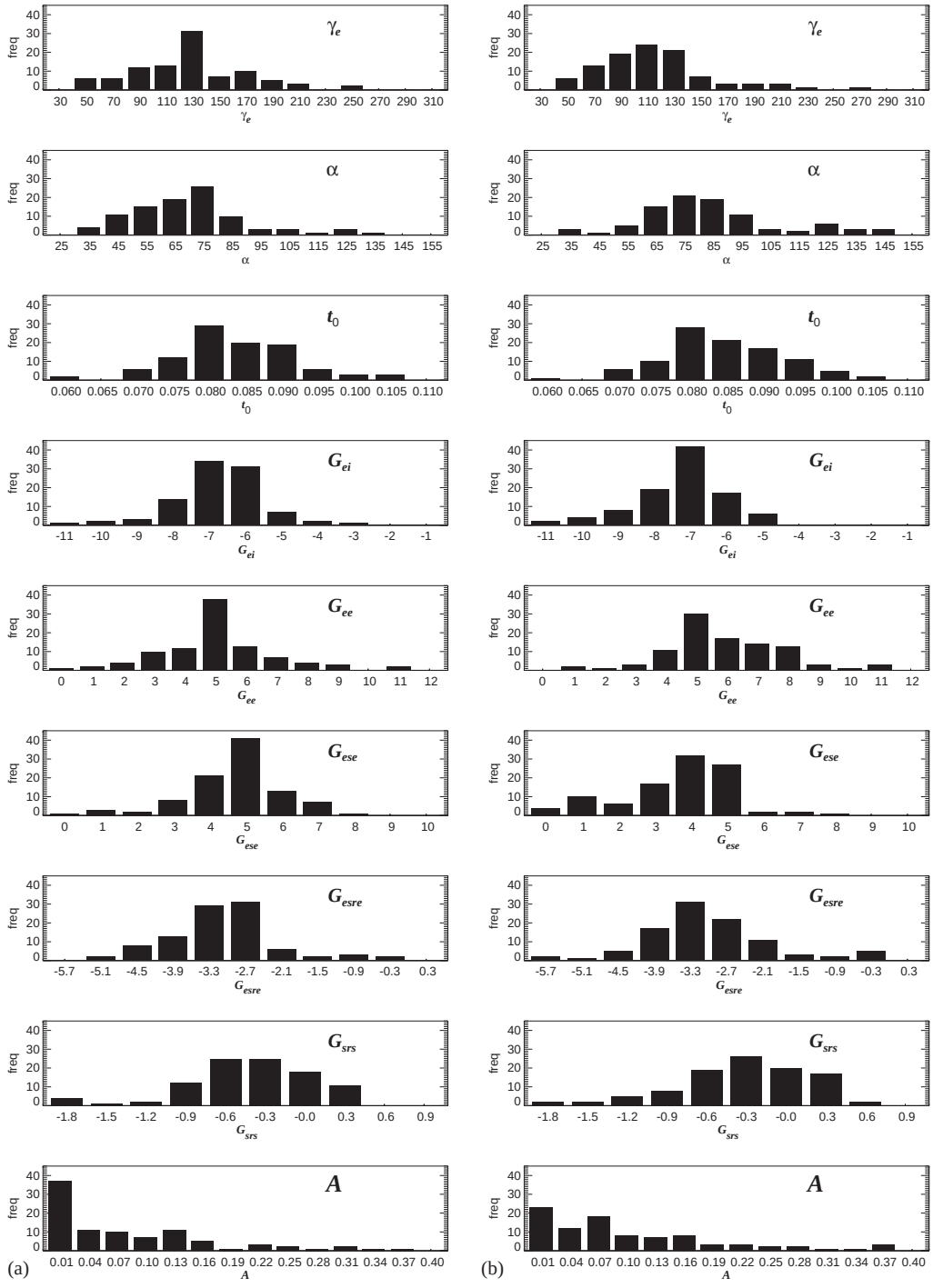

Fig. 5. Parameter distributions for 100 subjects for eyes-closed in column (i) and eyes-open in column (ii).

EMG parameter would significantly increase in the eyes-open condition given the relative increase in band power above 20 Hz (Table 3). However, as a reflection of sensory-related (e.g. eyes-open) neural activity, this change is ideally accounted for by the dendritic rate parameter α (Table 3). Therefore, using Wilcoxon Signed Ranks, the change in the EMG parameter between conditions was assessed. The slight increase in the eyes-open condition was not significant at $p<0.01$ ($p=0.048$ and $Z=1.98$), although there was a slight trend indicating its increase. Despite this, α remained highly significant across condition with $p<0.005$ (Table 3). This suggests these two parameters are relatively independent and that the EMG correction did not have a strong influence upon the estimate of the dendritic rate parameter α, most likely due to the

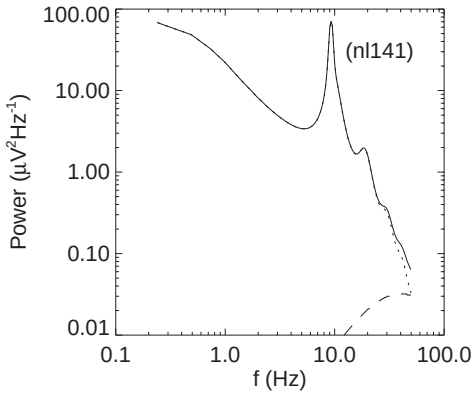

Fig. 6. Modeled spectrum for a subject's EEG data in the eyes-closed state showing subject number and the effects of EMG correction for a typical value of $A = 0.128\,\mu V^2/Hz$, with EMG (- - -), EEG (…) and EMG + EEG (—) spectral components. Note that only the spectrum above approximately 25 Hz is affected and the characteristic shape of the spectrum remains the same.

different frequency response characteristics of the EEG and EMG models.

5.2.3. qEEG values

The mean values for each *relative* band power of qEEG are listed in Table 3 for each state. The change in qEEG across state was also tested for significance using a paired-samples *t*-test. Relative band powers $P_\delta, P_\theta, P_{\beta 2}, P_{\beta 3}$, and $P\gamma$ were significantly larger in the eyes-open relative to the eyes-closed state, whereas P_α was significantly smaller. These results are consistent with typical findings regarding the transitions in EEG power between relaxed eyes-closed and eyes-open states (e.g. Niedermeyer and Lopes da Silva, 1999).

5.3. Difference correlations across state

Difference values were computed for each band power and model parameter, and a Pearson's correlation matrix was computed to compare associations between various changes in the model parameters and qEEG across state (Tables 4 and 5). For example, in Table 5 the value of $\alpha_{ec} - \alpha_{eo} = \Delta\alpha$, was correlated with $P_\alpha^{ec} - P_\alpha^{eo} = \Delta P\alpha$, and so forth.

5.3.1. EEG model parameters

From the model parameter interrelationships given in Table 4, three significant trends can be observed: (i) strong positive correlations between inhibitory and excitatory cortical ($\Delta|G_{ei}|$ and ΔG_{ee}) and thalamic gains (ΔG_{ese} and $\Delta|G_{esre}|$), (ii) positive correlations between the dendritic rate parameter α and cortical gains $\Delta|G_{ei}|$ and ΔG_{ee}, but (iii) negative correlations between α and the thalamic gain gains ΔG_{ese} and $\Delta|G_{srs}|$. These correlations illustrate (a) a balance between excitatory and inhibitory processes, (b) a positive association between cortical gains and the dendritic rate parameter, but a negative association with thalamic gains and the dendritic rate parameter, and (c) a reciprocal relationship between cortical gains ($|G_{ei}|$, G_{ee} and α), and thalamic gains (G_{ese} and $|G_{srs}|$).

5.3.2. EEG model parameters and qEEG

Table 5 illustrates the association between changes in the EEG model parameters and associated changes in qEEG relative band powers. Of particular interest are changes in the parameters α, G_{ese}, $|G_{esre}|$, and $|G_{srs}|$, and the associated changes in qEEG band powers. We expected each of these parameters to affect specific components of the spectra as illustrated in the parameter sensitivity plots (Fig. 3), and as supported by the correlation coefficients; (i) The higher dendritic rate parameter α was associated with a reduction in alpha band power, but an increase in slow wave and beta2−gamma band power. (2) The corticothalamic gain G_{ese} was opposite with an increase associated with an enhancement in α band power, but a reduction in Δ and θ band power. (3) Inhibitory corticothalamic gain $|G_{esre}|$ was associated with enhancements in θ band power. (4) Intrathalamic gain $|G_{srs}|$ was associated with an increase in theta and delta band power, but a decrease in alpha band power.

6. Discussion

In this paper we have generalized our recent biophysical model of the brain, and used it to infer physiological parameters underlying the waking EEG in 100 human subjects. This has allowed us to demonstrate the validity and reliability of the model, and its utility for probing physiology. The model fits show high accuracy (low-χ^2) and provide estimates of 'nominal' ranges for the physiological parameters underlying the spectral data. The entire experimental range (0.25–50 Hz) of spectral features from both the eyes-closed and eyes-open states, and the variability seen in the size of the alpha and beta peaks is all reproduced by the model (Fig. 4). The transitions in the parameters between each state and their predicted effects on the EEG spectra (Fig. 3) are also found to be consistent with the expected transitions in the qEEG measures (Table 3). However, unlike the band powers of the qEEG, the model parameters provide much more informative physiological information, particularly in terms of mechanisms of low-pass filtering and cortical modulation by resonant corticothalamic loops with either excitatory or inhibitory feedback characteristics.

The range of the physiological parameters from the model fits display relatively tight 'normal' distributions (Fig. 5) with few outliers, suggesting the model captures the individual variability occurring within the popula-

tion sample. With the exception of five subjects (probably affected by noise), these parameter values converged unconstrained (parameters were free to vary within a broad range) to what is considered within physiologically realistic limits. Values outside these ranges only lead to poor matches with the data (Rowe et al., 2002a, b) and/or instabilities resembling seizure (Robinson et al., 2002), implying the parameter values found in this study are far from arbitrary and are crucial for fitting waking states in the EEG. Furthermore, these values and other fixed parameters prove to be in good agreement with independent estimates as discussed below (e.g. Nunez, 2002; Rall, 1967; Thomson et al., 1996). Further research is required to identify the precise mechanisms and experimental values of physiology underlying the EEG, however this is the effort of current and future work, which provides further discussion of the links between the various parameters and underlying physiological processes (Robinson et al., 2004; Rowe et al., 2004a, b, c).

The physiological basis of the model is also consistent with the experimental and theoretical work of others (Freeman, 1975; Gill et al., 2002; Jirsa and Haken, 1996, 1997; Liley and Wright, 1994; Lopes da Silva et al., 1974; Lopes da Silva, 1999; Nunez, 1974, 1995b; Rennie et al., 1999; van Rotterdam et al., 1982; Wilson and Cowan, 1973; Wright and Liley, 1994, 1995). These other approaches are not aimed at fitting individual EEG spectra so there is no way for direct comparison between different models, without explicitly designing a model that is identical in every respect except for subcortical structures (e.g. hippocampus and associated synaptic interconnections versus thalamus). However, we have chosen a physiologically grounded approach that incorporates primary neural components in a

Table 4
Correlation matrix showing the relationship between parameter differences across state (highlighted, bolded values are significant at $p<.005$)

	$\Delta\gamma_e$	$\Delta\alpha$	Δt_0	$\Delta\lvert G_{ei}\rvert$	ΔG_{ee}	ΔG_{ese}	$\Delta\lvert G_{esre}\rvert$
$\Delta\alpha$	**−.300**						
Δt_0	−.006	.157					
$\Delta\lvert G_{ei}\rvert$	.216	**.378**	−.029				
ΔG_{ee}	.110	**.460**	.022	**.948**			
ΔG_{ese}	.062	**−.306**	.133	−.113	−.154		
$\Delta\lvert G_{esre}\rvert$	−.257	−.042	.208	−.185	−.083	**.784**	
$\Delta\lvert G_{srs}\rvert$	.229	**−.270**	−.029	.016	.164	.166	.182

Table 5
Correlation matrix comparing the relationship between changes in EEG model parameters and associated changes in relative band powers between eyes-closed and eyes-open states (highlighted, bolded values are significant at $p<.005$).

		EEG model parameters							
		$\Delta\gamma_e$	$\Delta\alpha$	Δt_0	$\Delta\lvert G_{ei}\rvert$	ΔG_{ee}	ΔG_{ese}	$\Delta\lvert G_{esre}\rvert$	$\Delta\lvert G_{srs}\rvert$
qEEG (relative power)	Δ_{slow}	**−.324**	**.411**	.166	**−.287**	**.384**	−.092	−.109	.258
	Δ_{delta}	**−.417**	.178	−.072	.136	−.062	**−.389**	−.012	**.329**
	Δ_{theta}	**−.273**	−.022	−.147	−.005	−.091	**−.372**	**.343**	**.294**
	Δ_{alpha}	**.506**	**−.478**	−.068	.073	−.156	**.447**	−.050	**−.413**
	Δ_{beta1}	.124	−.033	.074	.133	−.126	.004	−.069	−.205
	Δ_{beta2}	−.080	**.396**	−.045	.029	.040	−.192	.010	−.057
	Δ_{beta3}	−.085	**.348**	.103	.087	−.032	−.120	−.014	.120
	Δ_{gamma}	−.082	**.427**	.154	.016	.035	−.180	.038	.219

thalamocortical model. Such models incorporating the cortex and thalamus and experimental work examining thalamocortical activity, have indicated that these structures are essential components of various states of arousal and sensory processing (Bazhenov et al., 1998; Destexhe et al., 1994; Lumer et al., 1997a; McCormick and Bal, 1994, 1997; Steriade et al., 1997; Steriade, 2000; Timofeev et al., 1996). Therefore we have maintained this approach, rather than incorporating other structures such as the hippocampus, due to the broad physiological evidence that the current structures are essential.

6.1. Comparison of parameters with independent values

Measures of various physiological values underlying the activity of the human brain are difficult to obtain, with most estimates being based on animal data (e.g. Thomson et al., 1996). Furthermore, EEG measures in animals are not necessarily directly comparable to similar measures in humans. Part of our goal has been to extract values for physiological parameters that underlie the EEG in human brain function (Fig. 5). Many of these values and others in the model have been found to be consistent with independent measurements (Nunez, 1995b; Rall, 1967; Thomson et al., 1996) and theoretical estimates (Lumer et al., 1997a; Suffczynski et al., 2001; Wilson and Cowan, 1973). Lumer et al. (1997a) and Suffczynski et al. (2001) used experimental estimates of dendritic decay constants ranging from 2.4 to 40 ms for various neurons, in good agreement with the distribution of $1/\alpha$ in this study, ranging from 7 to 33 ms. Others have provided estimates of $10\,\mathrm{m\,s^{-1}}$ for the axonal conduction velocity of pyramidal neurons (Freeman and Baird, 1987; Nunez, 1995b), consistent with our mean value of $11\,\mathrm{m\,s^{-1}}$, calculated from $\gamma_e = 140\,s^{-1}$ (assuming a characteristic axonal range of 80 mm; (e.g. Braitenberg and Schüz, 1991; Nunez, 2002). Values for other parameters in the model including synaptic potentials for various neurons, values for G_{ab}, and other neural time constants are consistent with those in the literature (Nunez, 2002; Rall, 1967; Thomson et al., 1996; Thomson, 1997) and previous work (Rennie et al., 2000, 2002; Robinson et al., 1997, 2001b, 2002). Recent work has also inferred the corresponding neural firing rates and receptor activities (e.g. NMDA, AMPA, $GABA_A$) from the neural gains, consistent with the values here, and consistent with rates that are typical of experimental work measuring the firing activity of various neural populations (Robinson et al., 2004).

The EEG model is based on a quantification of the average properties of certain neural sub-populations, and inverse modeling allows values to be inferred for the parameters that characterize these sub-populations. These values, such as the gains G_{ab}, are combinations of factors (e.g. synaptic distributions on dendrites, cell subtypes, resting potentials, extracellular conditions) that are more fundamental. At this stage quantitative models of large-scale EEG do not explicitly incorporate all available neurophysiological details, although the most relevant are being incorporated in current and future work (Robinson et al., 2004). For now the bridge between quantifications and the ultimate mechanisms and fluctuations remains somewhat speculative, but provides ground work for future studies. It is with this context in mind that we consider in the following sections potential interpretation and significance of the model's physiological parameters.

6.2. Dendritic rate parameter α, cortical gains and sensory processing

An increase in sensory processing (i.e. eyes-open), relative to an absence of visual processing (i.e. eyes-closed), was associated with an increase in the dendritic rate parameter α and cortical gains G_{ee} and $|G_{ei}|$ (in this case, primarily that of excitatory cortical neurons G_{ee}, Table 3). α was also positively correlated with changes in cortical gains G_{ee} and $|G_{ei}|$ (Table 4). The EEG model predicts that increases in the dendritic rate parameters α and β (Table 2) result in spectral power enhancements above approximately 20 Hz by altering the low-pass filtering characteristics of the dendrites to expand their passband (Figs. 3(b and c) and Table 5). Psychophysiological studies indicate that such spectral enhancements are characteristic of increased cortical activation and/or sensory processing (Basar et al., 2001a; Engel and Singer, 2001; Herrmann, 2001; Jefferys et al., 1996). Given, the neural gains are a combination of average firing rates, and the number and response strength of synapses, the increased gains can therefore be inferred as an increase in the overall firing rates of cortical neurons and the corresponding synaptic activity. In terms of physiology, the increase in "synaptic background activity" can in turn result in a greater fraction of voltage-gated ion channels being open at any instant, causing a drop in average membrane resistance, and thus increasing the dendritic rate parameters (Koch, 1999, p. 416). A similar phenomenon has been observed by Ho and Destexhe (2000) where high amplitude fluctuations in membrane potential and faster dendritic time constants (effectively higher α and β) due to AMPA-mediated synapses lead to an enhancement in the responsiveness of pyramidal neurons.

6.3. Dendritic rate parameter α and thalamic activation

In contrast to the increase in cortical gains in the eyes-open state, the thalamic gains displayed an opposite trend; Changes in G_{ese} and $|G_{srs}|$ displayed strong *negative* correlations with Δalpha (Table 4), and were

significantly smaller in the eyes-open state. The change in G_{ese} was also positively correlated with changes in alpha band power, as predicted (Fig. 3(g)), but negatively correlated with changes in delta and theta band powers (Table 5). What this illustrates is a crucial functional distinction: decreased cortical gain or *idling* (e.g. relaxed eyes-closed), marked by strong alpha resonance, is associated with strong positive (excitatory, G_{ese}) corticothalamic feedback and lower dendritic rate parameters (i.e. longer dendritic time constants). In contrast, increased visual processing (e.g. eyes-open) marked by alpha *desynchronization* or *detuning* (representative of increased sensory processing) is associated with decreased corticothalamocortical gain, but higher dendritic rate parameters and increased cortical gains.

6.4. Intrathalamic activity and the TRN

The precise functional role of the TRN is complex, particularly during waking. Its function is better known during slow wave sleep, being implicated in conjunction with thalamocortical neurons in the generation of spindle oscillations and delta activity (Steriade et al., 1991). The slight increase in the intrathalamic gain $|G_{srs}|$ (including the TRN) in the eyes-closed state (Table 3) has only marginal influence upon the spectral shape of the EEG (Fig. 3(i)) and the TRN is not the generator of the alpha resonance characteristic of this state. However, sufficient increase in $|G_{srs}|$ (well above the waking levels found here), in combination with sufficient negative corticothalamic gain $|G_{esre}|$ (rather than positive G_{ese}) will lead to the enhancement of $\Delta-\theta$, and spindle resonances characteristic of slow wave sleep (Rennie et al., 2002; Robinson et al., 2002).

6.5. Cortical idling and alpha tuning

The apparent widespread synchrony of the alpha rhythm across the cortex (e.g. eyes-closed) is often referred to as *cortical idling* (Pfurtscheller, 1992; for a review see Pfurtscheller et al., 1996, 1994), and mechanisms underlying alpha activity have been suggested to involve thalamocortical circuitry (Danos et al., 2001; Fanselow et al., 2001; Isaichev et al., 2001; Larson et al., 1998; Lopes da Silva, 1991; Lopes da Silva et al., 1997; Nicolelis et al., 1995; Pritchard and Duke, 1997; Semba et al., 1980; Semba and Komisaruk, 1984; Suffczynski et al., 2001). Here, this involves high positive corticothalamic feedback G_{ese} that modulates the activity of neural fields ϕ_e in the cortex, as supported by predictions (Fig. 3(g)) and experimental results; a strong correlation between alpha power and G_{ese}, and the significant increase in this parameter (eyes-closed) in the presence of strong alpha rhythm (Table 3). Specifically, increased G_{ese} has the effect of amplifying and sharpening (*tuning*) the resonance of ϕ_e to a frequency ($\sim$10 Hz) approximately equal to the inverse of the total corticothalamic loop delay time t_0 (Robinson et al., 2001b). This resonance is strongest in large spatial scale activity and thus appears as 'synchronous' alpha rhythm. The functional significance of this rhythm may be as a mechanism which periodically modulates the mean membrane potential over a large area of the cortex (Lopes da Silva, 1991; Williamson et al., 1997), presumably favoring 'non-specific' and broad cortical activation (idling), rather than 'focal' activation and suppression (Crick, 1984; Le Masson et al., 2002; McCormick and Bal, 1994; Yingling and Skinner, 1976).

6.6. α detuning (desynchronization)

The effect of alpha detuning is to reduce the dominance of the peak alpha frequency, leading to a more irregular time series, in what is commonly termed "alpha desynchronization". This phenomenon occurs in the model as positive corticothalamic feedback G_{ese} decreases and the proportion of negative corticothalamic feedback G_{esre} increases, as found in the transition from eyes-closed to eyes-open. The resultant effects on the net gain of neocortical fields are complicated (see Robinson et al., 2001b, for details); however, in summary, what occurs is a *detuning* of the alpha resonance, with possible enhancement of delta–theta resonance depending on the relative strength of G_{esre} over G_{ese}. As indicated in predictions (Figs. 3(g and h)), and further supported by the experimental results with positive correlations between low frequency (delta and theta) resonances and G_{esre}, and by negative correlations between low frequency resonances and G_{ese} (Table 5). Presumably, this phenomenon is a reflection of variant positive and negative corticothalamic feedback that is required to relay signals to specific cortical regions in response to incoming sensory stimuli (Crick, 1984; Stehberg et al., 2001; Weese et al., 1999; Yingling and Skinner, 1976).

It is important to note that the theta mentioned here is not necessarily related to hippocampal theta oscillations commonly measured in animals (e.g. Buzsaki et al., 2003; Williams and Givens, 2003). The origins of cortical theta in human EEG remains uncertain (Molle et al., 2002), although studies do demonstrate that both human scalp and animal hippocampal theta are related to similar cognitive processes (Hasselmo et al., 2002; Klausberger et al., 2003; Klimesch, 1996, 1999), and may occur due to increased activity in cortico-hippocampal feedback loops (Buzsaki, 1996; Kahana et al., 1999). We have offered an explanation that is specific to the delta–theta enhancements (not narrow-band theta oscillations) that occur in the human EEG, particularly during states of reduced arousal and slow wave sleep. This relates to activity in corticothalamic loops, primarily due to the negative corticothalamic pathway

(G_{esre}, Fig. 3(h)) involving the TRN (Rennie et al., 2002; Robinson et al., 2002). During alert states involving sensory processing this delta–theta resonance is expected to be more variable, rather than the 'clock' like delta activity found during the early stages of sleep, but also found to be due to mechanisms involving thalamocortical cells and the TRN (Amzica and Steriade, 1998; Steriade et al., 1991, 1993).

6.7. Cortical stability and excitatory and inhibitory processes

The balance between the inhibitory and excitatory processes in the cortex is thought to function as a way of maintaining cortical stability and firing rates within certain boundaries (e.g. Jonas et al., 1998; Varela et al., 1999). Consistent with this proposal, we found very strong positive correlations between inhibitory and excitatory cortical gains ($r = 0.948$), and between inhibitory and excitatory thalamic gains ($r = 0.784$, Table 4). The balance between excitatory G_{ee} and inhibitory G_{ei} closely influences the $1/f$ spectral component (0–5 Hz) of the EEG (Figs. 4(d and e)). Implying that the cortical gains and this spectral range (traditionally considered as $1/f$ "noise" and ignored in EEG studies) can provide an index of cortical stability, since such spectra are known to characterize systems close to marginal stability (Robinson et al., 2001b).

The $1/f$ characteristic is typically more prominent in the 'relaxed' eyes-closed spectra or 'idling' state, suggesting 'marginal' stability (Fig. 4). This state of broad non-focal activation is consistent with the prior suggestion that the alpha rhythm (characteristic of the eyes-closed state) may set the average membrane potential over a large area of cortex (Lopes da Silva, 1991; Williamson et al., 1997), thereby affecting neural flexibility and the responsiveness of the networks. In contrast, when networks undergo focal activation and suppression in response to sensory stimuli (Crick, 1984; Stehberg et al., 2001; Weese et al., 1999; Yingling and Skinner, 1976), their dedicated network activities may lead to greater cortical stability, as suggested by the flatter $1/f$ spectra in the eyes-open state. Note also that the *local* inhibitory intracortical gain $|G_{ei}|$ is larger than excitatory cortical gain G_{ee} in both states, but particularly the eyes-open (Table 3). An increase in the proportion of $|G_{ei}|$ will tend to lead to flatter $1/f$ spectra (Fig. 3(d)) or increased stability. This suggests that in the absence of thalamic effects, the cortex would always be under constant net inhibition, particularly during sensory processing, thus preventing instabilities associated with abnormal excitatory cortical gain. In terms of the thalamus, the balance between inhibitory $|G_{esre}|$ and excitatory G_{ese} corticothalamic gain is also crucial for cortical stability. We have previously shown that sufficient deviations of the balance between thalamic gains from the nominal physiological ranges can result in spike and wave form like activity that closely resembles seizure in epilepsy (Robinson et al., 2002).

6.8. Role of cortical damping γ_e

The moderate change in cortical damping γ_e between states found in this study appears anomalous since this parameter is proportional to the relatively constant axonal conduction velocity v_e (dependent primarily on axon diameter and the degree of myelination), and inversely proportional to the characteristic axonal range r_e. It is possible that changes in neurochemical concentrations lead to moderate changes in axonal velocity and, hence, in γ_e. We are not aware of any findings directly relating to this point, but such an effect is well known under halothane anesthesia, with associated reductions in v_e and suppression of alpha band activity (Katznelson, 1981; Nunez, 1995a, b). We also do not find any evidence for a corresponding change in t_0, which would be expected if v_e were altered, although we do find that reductions in γ_e (i.e. v_e) are associated with reduced alpha resonance (Fig. 3(a), Tables 3 and 5).

Alternatively, the change in γ_e may be an artefact resulting from incomplete separation by the fitting routine of its effects from similar ones resulting from other parameters (Fig. 3). Supporting this interpretation, γ_e appears to have a much tighter distribution for the eyes-closed condition, suggesting it may be better determined during this state (Fig. 5). If this is correct, this parameter could be constrained to have the same value in other states for each subject, thereby separating its effects from those of other variables more fully; however, initial investigations imply that this does not change the other parameters by large amounts, so we do not pursue it here.

In contrast to the between-states situation, there are strong reasons to expect γ_e to change developmentally. Myelination, in particular, increases during development, leading to higher conduction velocity. Similarly, the spatial extent of axonal projections is also likely to change as a function of development with the occurrence of both neural pruning and network formation. This leads us to expect significant developmental effects, which we will investigate in future work, and for example, is also consistent with the increase in the α frequency in childhood (e.g. Niedermeyer and Lopes da Silva, 1999).

7. Conclusion

We have used our recently developed biophysical model of the brain that has been successfully used to fit EEG spectra from 100 human subjects. The model fits have enabled values for the underlying physiological

parameters to be determined, and these values are consistent with known independent experimental measurements. Moreover, the parameters provide an understanding of the EEG spectra in terms of mechanisms of low-pass filtering and cortical modulation by resonant corticothalamic loops: Dendritic filtering and cortical damping contribute primarily to the overall shape of the spectra, while the corticothalamic resonances contribute primarily to spectral peaks and troughs. Thus, high dendritic rate parameters and increased cortical gains (but decreased thalamic gains) are associated with sensory processing and a *detuning* ('desynchronization') of the alpha resonance; Whereas low dendritic rate parameters and decreased cortical gains (but increased thalamic gains) are associated with states of *cortical idling* and *tuning* ('synchronization') of the alpha resonance.

Here and in previous papers, we have presented a general theory of brain activity that is consistent with other established large-scale neural models (Lopes da Silva and Mesulam, 1990; Lumer et al., 1997a, b; Suffczynski et al., 1999, 2001) and more detailed descriptions of neural phenomena (Basar et al., 2001b; Brunia, 2001; Destexhe et al., 1998a; LaBerge, 2001; Nunez et al., 2001; Steriade et al., 1990). The present work improves both quantitatively and qualitatively upon previous modeling because, for the first time, the model is used to explicitly estimate the values of the underlying neurophysiological parameters using a large database of human EEG spectra. The number of neurophysiological parameters and the degree of neural structure incorporated has also been optimized so that details that do not impact on the variance of the data have been removed, but close prediction of the important properties of the data has still been achieved (Section 2.3 and 4.1). This had the effect of maximizing the discriminatory power of the model parameters.

Some readers may still criticize the number of 'free' parameters. However, note that the model does not contain 'free' parameters in the usual sense. Instead the model parameters are strongly constrained by physiology (Robinson et al., 2004), separately from the requirement that they must produce an accurate fit to the EEG spectrum. Furthermore, other biophysical EEG models in the literature as described in references, have many more parameters.

We also note that the electrophysiological responses examined in this paper are that of 'tonic' baseline activity in the EEG rather than the 'phasic' EEG activity apparent in the examination of event-related potentials (ERPs). The latter incorporates more complex temporal cortical dynamics, as discussed in Rennie et al. (2002). However, the current study of 'tonic' cortical mechanisms has allowed us to provide a baseline of 'nominal' cortical functioning in terms of the model parameters, which is essential to underpin work on more complicated states (Rowe et al., 2004a, b, c). As an initial study modeling experimental data, we have also only examined parameter transitions at a single scalp site. However we do expect certain parameters such as t_0 to vary across the scalp, indicating the necessity to model spatial inhomogeneities (O'Connor et al., 2002; O'Connor and Robinson, 2003; Robinson et al., 2003b). In future work we aim to apply the same principles and methodology to multiple scalp sites and the analysis and quantification of varying states of arousal in healthy subjects (Rowe et al., 2002b) and patients with sleep, arousal, and other abnormalities (Rowe et al., 2004a, b, c), and to ERPs (Rennie et al., 2002). As well as possibly incorporating spatial inhomogeneities (O'Connor et al., 2002; O'Connor and Robinson, 2003; Robinson et al., 2003b) and the convoluted geometry of the cortex.

Acknowledgements

This work was supported by a University of Sydney Sesqui Grant. The authors wish to thank Michael Breakspear and Evian Gordon for helpful discussions and comments, and Homi Bahramali and Illario Lazzaro for their contributions to the EEG database of 100 healthy subjects that was used in this study.

References

Amzica, F., Steriade, M., 1998. Electrophysiological correlates of sleep delta waves. Electroencephalography Clin. Neurophysiol. 107 (2), 69–83.

Anderson, J.A., 1995. An Introduction to Neural Networks. MIT Press, Cambridge, MA.

Bahramali, H., Gordon, E., Lim, C.L., Li, W., Lagopoulos, J., Leslie, J., Rennie, C., Meares, R.A., 1997. Evoked related potentials associated with and without an orienting reflex. Neuroreport 8 (12), 2665–2669.

Bahramali, H., Gordon, E., Li, W.M., Rennie, C., Wright, J., 1998. Fast and slow reaction time changes reflected in ERP brain function. Int. J. Neurosci. 93 (1–2), 75–85.

Bahramali, H., Gordon, E., Lagopoulos, J., Lim, C.L., Li, W., Leslie, J., Wright, J., 1999. The effects of age on late components of the ERP and reaction time. Exp. Aging Res. 25 (1), 69–80.

Basar, E., Basar-Eroglu, C., Karakas, S., Schurmann, M., 2001a. Gamma, alpha, delta, and theta oscillations govern cognitive processes. Int. J. Psychophysiol. 39, 241–248.

Basar, E., Schurmann, M., Sakowitz, O., 2001b. The selectively distributed theta system: functions. Int. J. Psychophysiol. 39, 197–212.

Bazhenov, M., Timofeev, I., Steriade, M., Sejnowski, T.J., 1998. Computational models of thalamocortical augmenting responses. J. Neurosci. 18 (16), 6444–6465.

Braitenberg, V., Schüz, A., 1991. Anatomy of the Cortex: Statistics and Geometry. Springer, Berlin.

Brunia, C.H., 2001. Thalamo-cortical relations in attention and consciousness. Int. J. Psychophysiol. 43 (1), 1–4.

Bullier, J., Henry, G.H., 1979. Neural path taken by afferent streams in striate cortex of the cat. J. Neurophysiol. 42 (5), 1264–1270.

Buzsaki, G., 1996. The hippocampo-neocortical dialogue. Cereb. Cortex 6 (2), 81–92.

Buzsaki, G., Buhl, D.L., Harris, K.D., Csicsvari, J., Czeh, B., Morozov, A., 2003. Hippocampal network patterns of activity in the mouse. Neuroscience 116 (1), 201–211.

Crick, F., 1984. Function of the thalamic reticular nucleus: the searchlight hypothesis. Proc. Natl Acad. Sci. 81, 4586–4590.

Croft, R.J., Barry, R.J., 2000. EOG correction: which regression should we use? Psychophysiology 37 (1), 123–125.

Danos, P., Guich, S., Abel, L., Buchsbaum, M.S., 2001. Eeg alpha rhythm and glucose metabolic rate in the thalamus in schizophrenia. Neuropsychobiology 43 (4), 265–272.

Destexhe, A., Contreras, D., Sejnowski, T.J., Steriade, M., 1994. A model of spindle rhythmicity in the isolated thalamic reticular nucleus. J. Neurophysiol. 72 (2), 803–818.

Destexhe, A., Contreras, D., Steriade, M., 1998a. Mechanisms underlying the synchronizing action of corticothalamic feedback through inhibition of thalamic relay cells. J. Neurophysiol. 79 (2), 999–1016.

Destexhe, A., Mainen, Z.F., Sejnowski, T., 1998b. Kinetic models of synaptic transmission. In: Koch, C., Segev, I. (Eds.), Methods in Neuronal Modeling. MIT Press, Cambridge, MA, pp. 1–25.

Destexhe, A., Mainen, Z.F., Sejnowski, T., 2002. Kinetic models for synaptic interactions. In: Arbib, M.A. (Ed.), The Handbook of Brain Theory and Neural Networks. MIT Press, Cambridge, MA, pp. 1126–1130.

Dinse, H.R., Kruger, K., 1994. The timing of processing along the visual pathway in the cat. Neuroreport 5 (8), 893–897.

Elman, J.L., 1995. Language as a dynamical system. In: Port, R.F., van Gelder, T. (Eds.), Mind as Motion: Explorations in the Dynamics of Cognition. MIT Press, Cambridge, MA, pp. 195–225.

Engel, A.K., Singer, W., 2001. Temporal binding and the neural correlates of sensory awareness. Trends in Cognitive Sciences 5 (1), 16–25.

Fanselow, E.E., Sameshima, K., Baccala, L.A., Nicolelis, M.A., 2001. Thalamic bursting in rats during different awake behavioral states. Proc. Natl Acad. Sci. USA 98 (26), 15330–15335.

Freeman, W.J., 1975. Mass action in the nervous system. Academic Press, New York, NY.

Freeman, W.J., 1987. Simulation of chaotic EEG patterns with a dynamic model of the olfactory system. Biol. Cybernet. 56 (2–3), 139–150.

Freeman, W.J., 2003. Evidence from human scalp electroencephalograms of global chaotic itinerancy. Chaos 13 (3), 1067–1077.

Freeman, W.J., Baird, B., 1987. Relation of olfactory EEG to behavior: spatial analysis. Behav. Neurosci. 101, 393–408.

Freeman, W.J., Rogers, L.J., 2002. Fine temporal resolution of analytic phase reveals episodic synchronization by state transitions in gamma EEGs. J. Neurophysiol. 87 (2), 937–945.

Gill, P.R., Murray, W., Wright, M.H., 2002. The Levenberg–Marquardt Method. In: Wright, M.H., Gill, P.R. (Eds.), Practical Optimization. Academic Press, London, pp. 136–137.

Gluck, M.A., Glauthier, P.T., Sutton, R.S., 1992. Adaptation of cue-specific learning rates in network models of human category learning. Proceedings of the 14th Annual Conference of the Cognitive Science Society (Bloomington, IN), Lawrence Erlbaum., Hillsdale, NJ, pp. 540–545.

Gordon, E., 2000. Integrative neuroscience: the big picture. In: Gordon, E. (Ed.), Integrative Neuroscience: Bringing together Biological, Psychological and Clinical Models of the Human Brain. Harwood Academic Publishers, Amsterdam, The Netherlands, pp. 1–28.

Gratton, G., Coles, M., Donchin, E., 1983. A new method for off-line removal of ocular artifact. Electroencephalogr. Clin. Neurophysiol. 55, 468–484.

Hasselmo, M.E., Hay, J., Ilyn, M., Gorchetchnikov, A., 2002. Neuromodulation, theta rhythm and rat spatial navigation. Neural Networks 15 (4–6), 689–707.

Herrmann, C.S., 2001. Gamma activity in human EEG is related to high speed memory comparisons during object selective attention. Vis. Cognition 8 (3/4/5), 593–608.

Ho, N., Destexhe, A., 2000. Synaptic background activity enhances the responsiveness of neocortical pyramidal neurons. J. Neurophysiol. 84 (3), 1488–1496.

Isaichev, S.A., Derevyankin, V.T., Koptelov, Y., Sokolov, E.N., 2001. Rhythmic alpha-activity generators in the human EEG. Neurosci. Behav. Physiol. 31 (1), 49–53.

Jefferys, J.G., Traub, R.D., Whittington, M.A., 1996. Neuronal networks for induced '40 Hz' rhythms. Trends Neurosci. 19 (5), 202–208.

Jirsa, V.K., Haken, H., 1996. Field theory of electromagnetic brain activity. Phys. Rev. Lett. 77, 960–963.

Jirsa, V.K., Haken, H., 1997. A derivation of a macroscopic field theory of the brain from the quasi-microscopic neural dynamics. Physica D 99, 503–526.

Jonas, P., Haverkampf, K., Kraushaar, U., Geiger, J.R.P., 1998. Glutamate- and GABA-mediated synaptic transmission in the principal neuron-interneuron network of the dentate gyrus. J. Physiol.—Proc. 511P (19S), 16.

Joyce, C.A., Gorodnitsky, I.F., Kutas, M., Kutas, M., 2004. Automatic removal of eye movement and blink artifacts from EEG data using blind component separation. Psychophysiology 41 (2), 313–325.

Kahana, M.J., Sekuler, R., Caplan, J.B., Kirschen, M., Madsen, J.R., 1999. Human theta oscillations exhibit task dependence during virtual maze navigation. Nature 399 (6738), 781–784.

Katznelson, R.D., 1981. Normal modes of the brain: neuroanatomical basis and a physiological and theoretical model. In: Nunez, P.L. (Ed.), Electric fields of the brain: the neurophysics of EEG. Oxford University Press, New York, pp. 401–437.

Kim, U., Sanchez-Vives, M.V., McCormick, D.A., 1997. Functional dynamics of GABAergic inhibition in the thalamus. Science 278 (5335), 130–134.

Klausberger, T., Magill, P.J., Marton, L.F., Roberts, J.D., Cobden, P.M., Buzsaki, G., Somogyi, P., 2003. Brain-state- and cell-type-specific firing of hippocampal interneurons in vivo. Nature 421 (6925), 844–848.

Klimesch, W., 1996. Memory processes, brain oscillations and EEG synchronization. Int. J. Psychophysiol. 24 (1–2), 61–100.

Klimesch, W., 1999. EEG alpha and theta oscillations reflect cognitive and memory performance: a review and analysis. Brain Res. Rev. 29 (2–3), 169–195.

Koch, C., 1999. Biophysics of Computation: Information Processing in Single Neurons. Oxford University Press, New York, NY.

LaBerge, D., 2001. Attention, consciousness, and electrical wave activity within the cortical column. Int. J. Psychophysiol. 43 (1), 5–24.

Larson, C.L., Davidson, R.J., Abercrombie, H.C., Ward, R.T., Schaefer, S.M., Jackson, D.C., Holden, J.E., Perlman, S.B., 1998. Relations between PET-derived measures of thalamic glucose metabolism and EEG alpha power. Psychophysiology 35 (2), 162–169.

Lazzaro, I., Gordon, E., Whitmont, S., Plahn, M., Li, W., Clarke, S., Dosen, A., Meares, R., 1998. Quantified EEG activity in adolescent attention deficit hyperactivity disorder. Clin. Electroencephalogr. 29 (1), 37–42.

Le Masson, G., Renaud-Le Masson, S., Debay, D., Bal, T., 2002. Feedback inhibition controls spike transfer in hybrid thalamic circuits. Nature 417 (6891), 854–858.

Lehmann, D., 1971. Multichannel topography of human alpha EEG fields. Electroencephalogr. Clin. Neurophysiol. 31 (5), 439–449.

Liley, D.T.J., Wright, J.J., 1994. Intracortical connectivity of pyramidal and stellate cells: estimates of synaptic densities and coupling symmetry. Network 5, 175–189.

Lopes da Silva, F.H., 1991. Neural mechanisms underlying brain waves: from neural membranes to networks. Electroencephalogr. Clin. Neurophysiol. 79 (2), 81–93.

Lopes da Silva, F.H., 1999. Dynamics of EEGs as signals of neuronal populations: models and theoretical considerations. In: Niedermeyer, E., Lopes da Silva, F.H. (Eds.), Electroencephalography: Basic Principles, Clinical Applications, and Related Fields. Williams & Watkins, Baltimore, MA, pp. 76–92.

Lopes da Silva, F.H., Hoeks, A., Smits, A., Zetterberg, L.H., 1974. Model of brain rhythmic activity: the alpha-rhythm of the thalamus. Kybernetik 15, 27–37.

Lopes da Silva, F.H., Mesulam, M.M., 1990. Basic mechanisms of cerebral rhythmic activities. Electroencephalogra. Clin. Neurophysiol. 76, 481–508.

Lopes da Silva, F.H., Pijn, J.P., Velis, D., Nijssen, P.C., 1997. Alpha rhythms: noise, dynamics and models. Int. J. Psychophysiol. 26 (1–3), 237–249.

Lumer, E.D., Edelman, G.M., Tononi, G., 1997a. Neural dynamics in a model of the thalamocortical system. I. Layers, loops and the emergence of fast synchronous rhythms. Cereb. Cortex 7 (3), 207–227.

Lumer, E.D., Edelman, G.M., Tononi, G., 1997b. Neural dynamics in a model of the thalamocortical system. II. The role of neural synchrony tested through perturbations of spike timing. Cereb. Cortex 7 (3), 228–236.

Martinovic, Z., Jovanovic, V., Ristanovic, D., 1998. EEG power spectra of normal preadolescent twins. Gender differences of quantitative EEG maturation. Neurophysiol. Clin. 28 (3), 231–248.

McCormick, D.A., Bal, T., 1994. Sensory gating mechanisms of the thalamus. Curr. Opin. Neurobiol. 4 (4), 550–556.

McCormick, D.A., Bal, T., 1997. Sleep and arousal: thalamocortical mechanisms. Annu. Rev. Neurosci. 201, 85–215.

Molle, M., Marshall, L., Fehm, H.L., Born, J., 2002. EEG theta synchronization conjoined with alpha desynchronization indicate intentional encoding. Eur. J. Neurosci. 15 (5), 923–928.

Nicolelis, M.A., Baccala, L.A., Lin, R.C., Chapin, J.K., 1995. Sensorimotor encoding by synchronous neural ensemble activity at multiple levels of the somatosensory system. Science 268 (5215), 1353–1358.

Niedermeyer, E., Lopes da Silva, F.H., 1999. Electroencephalography: Basic Principles, Clinical Applications and Related Fields. Williams & Watkins, Baltimore.

Nunez, P.L., 1974. Wave-like properties of the alpha rhythm. IEEE Trans. Biomed. Eng. 21, 473–482.

Nunez, P.L., 1995a. Continuous linear systems of physics and brain. In: Nunez, P.L. (Ed.), Neocortical Dynamics and Human EEG Rhythms. Oxford University Press, New York, pp. 369–416.

Nunez, P.L., 1995b. Neocortical Dynamics and Human EEG Rhythms. Oxford University Press, New York.

Nunez, P.L., 2002. Electric Fields of the Brain: the Neurophysics of EEG. Oxford University Press, Oxford, UK.

Nunez, P.L., Wingeier, B.M., Silberstein, R.B., 2001. Spatial–temporal structures of human alpha rhythms: theory, microcurrent sources, multiscale measurements, and global binding of local networks. Human Brain Mapping 13, 125–164.

O'Connor, S.C., Robinson, P.A., 2003. Wave-number spectrum of electrocorticographic signals. Phys. Rev. E 67, 051912

O'Connor, S.C., Robinson, P.A., Chiang, A.K.I., 2002. Wave-number spectrum of electroencephalographic signals. Phys. Rev. E 66, 061905.

Omori, M., Koshino, Y., Murata, T., Murata, I., Nishio, M., Sakamoto, K., Horie, T., Isaki, K., 1995. Quantitative EEG in never-treated schizophrenic patients. Biol. Psychiatry 38 (5), 305–309.

Pfurtscheller, G., 1992. Event-related Synchronization (ERS): an Electrophysiological Correlate of Cortical Areas at Rest. Electroencephalogr. Clin. Neurophysiol. 83 (1), 62–69.

Pfurtscheller, G., Neuper, C., 1994. Event-related synchronization of mu rhythm in the EEG over the cortical hand area in man. Neurosci. Lett. 174 (1), 93–96.

Pfurtscheller, G., Stancak Jr., A., Neuper, C., 1996. Event-related synchronization (ERS) in the alpha band–an electrophysiological correlate of cortical idling: a review. Int. J. Psychophysiol. 24 (1–2), 39–46.

Press, W.H., Teukolsky, S.A., Vertterling, W.T., Flannery, B.P., 1992. Numerical Recipes in C. Cambridge University Press, Cambridge, NY.

Pritchard, W.S., Duke, D.W., 1997. Segregation of the thalamic alpha rhythms from cortical alpha activity using the Savit-Green S-statistic and estimated correlation dimension. Int. J. Psychophysiol. 26 (1–3), 263–271.

Rall, W., 1967. Distinguishing theoretical synaptic potentials computed for different soma-dendritic distributions of synaptic input. J. Neurophysiol. 30 (5), 1138–1168.

Rennie, C.J., Robinson, P.A., Wright, J.J., 1999. Effects of local feedback on dispersion of electrical waves in the cerebral cortex. Phys. Rev. E 59 (3), 3320–3330.

Rennie, C.J., Wright, J.J., Robinson, P.A., 2000. Mechanisms of cortical electrical activity and the emergence of gamma rhythm. J. Theor. Biol. 205, 17–35.

Rennie, C.J., Robinson, P.A., Wright, J.J., 2002. Unified neurophysiological model of EEG spectra and evoked potentials. Biol. Cybern. 86 (6), 457–471.

Robinson, P.A., 2003. Neurophysical theory of coherence and correlations of electroencephalographic and electrocorticographic signals. J. Theor. Biol. 222 (2), 163–175.

Robinson, P.A., Rennie, C.J., Wright, J.J., 1997. Propagation and stability of waves of electrical activity in the cerebral cortex. Phys. Rev. E 56, 826–840.

Robinson, P.A., Rennie, C.J., Wright, J.J., Bourke, P.D., 1998. Steady states and global dynamics of electrical activity in the cerebral cortex. Phys. Rev. E 58, 3557–3571.

Robinson, P.A., Loxley, P.N., O'Connor, S.C., Rennie, C.J., 2001a. Modal analysis of corticothalamic dynamics, electroencephalographic spectra, and evoked potentials. Phys. Rev. E 63 (041909), 1–13.

Robinson, P.A., Rennie, C.J., Wright, J.J., Bahramali, H., Gordon, E., Rowe, D.L., 2001b. Prediction of electroencephalographic spectra from neurophysiology. Phys. Rev. E 63 (021903), 1–18.

Robinson, P.A., Rennie, C.J., Rowe, D.L., 2002. Dynamics of large-scale brain activity in normal arousal states and epileptic seizures. Phys. Rev. E 65 (041924), 1–9.

Robinson, P.A., Rennie, C.J., Rowe, D.L., O'Connor, S.C., Wright, J.J., Gordon, E., Whitehouse, R.W., 2003a. Neurophysical modeling of brain dynamics. Neuropsychopharmacology 28, S74–S79.

Robinson, P.A., Whitehouse, R.W., Rennie, C.J., 2003b. Nonuniform corticothalamic continuum model of EEG spectra with application to split-alpha peaks. Phys. Rev. E 68, 021922

Robinson, P.A., Rennie, C.J., Rowe, D.L., O'Connor, S.C., 2004. Estimation of neurophysiological of multiscale neurophysiological parameters by EEG means. Human Brain Mapping 23 (1), 53–72.

Rowe, D.L., Robinson, P.A., Rennie, C.J., Gordon, E., 2001. A model of electrophysiological spectra (EEG) in schizophrenia. Schizophr. Res. 41 (1), 208.

Rowe, D.L., Rennie, C.J., Wright, J.J., Robinson, P.A., Gordon, E., 2002a. Neurochemical mechanisms of theta, P2 & P3 abnormalities

in attention deficit hyperactivity disorder (ADHD). Int. J. Psychophysiol. 45 (1–2), 75–76.

Rowe, D.L., Robinson, P.A., Rennie, C.J., Gordon, E., 2002b. Modelling global brain dynamics in sleep & waking. Int. J. Psychophysiol. 45 (1–2), 76.

Rowe, D.L., Robinson, P.A., Harris, A.W., Felmingham, K.L., Lazzaro, I., 2004a. Neurophysiological modelling of tonic cortical activity in Post-traumatic Stress Disorder (PTSD), chronic schizophrenia, First Episode Schizophrenia (FESz) and Attention Deficit Hyperactivity Disorder (ADHD). J. Integrative Neurosci., in press.

Rowe, D.L., Robinson, P.A., Gordon, E., 2004b. Stimulant Drug Action in Attention Deficit Hyperactivity Disorder (ADHD): Inference of Neurophysiological Mechanisms via Quantitative Modelling. Clin. Neurophysiol., in press.

Rowe, D.L., Robinson, P.A., Lazzaro, I., Williams, L.M., 2004c. Biophysical modelling of tonic measures of cortical activity (EEG) in Attention Deficit Hyperactivity Disorder (ADHD). Int. J. Psychophysiol. submitted manuscript.

Rumelhart, D.E., 1989. The architecture of mind: a connectionist approach. In: Posner, M. (Ed.), Foundations of Cognitive Science. MIT Press, Cambridge, MA, pp. 133–159.

Rumelhart, D.E., McClelland, J.L., 1986. Parallel Distributed Processing: Explorations in the Microstructure of Cognition. MIT Press, Cambridge, MA.

Semba, K., Komisaruk, B.R., 1984. Neural substrates of two different rhythmical vibrissal movements in the rat. Neuroscience 12 (3), 761–774.

Semba, K., Szechtman, H., Komisaruk, B.R., 1980. Synchrony among rhythmical facial tremor, neocortical 'alpha' waves, and thalamic non-sensory neuronal bursts in intact awake rats. Brain Res. 195 (2), 281–298.

Shwedyk, E., Balasubramanian, R., Scott, R.N., 1977. A nonstationary model for the electromyogram. IEEE Trans. Biomed. Eng. 24 (5), 417–424.

Stehberg, J., Acuna-Goycolea, C., Ceric, F., Torrealba, F., 2001. The visceral sector of the thalamic reticular nucleus in the rat. Neuroscience 106 (4), 745–755.

Steriade, M., 2000. Corticothalamic resonance, states of vigilance and mentation. Neuroscience 101 (2), 243–276.

Steriade, M., Gloor, P., Llinas, R.R., Lopes de Silva, F.H., Mesulam, M.M., 1990. Basic mechanisms of cerebral rhythmic activities. Electroencephalogr. Clin. Neurophysiol. 76 (6), 481–508.

Steriade, M., Dossi, R.C., Nunez, A., 1991. Network modulation of a slow intrinsic oscillation of cat thalamocortical neurons implicated in sleep delta waves: cortically induced synchronization and brainstem cholinergic suppression. J. Neurosci. 11 (10), 3200–3217.

Steriade, M., Nunez, A., Amzica, F., 1993. Intracellular analysis of relations between the slow (<1 Hz) neocortical oscillation and other sleep rhythms of the electroencephalogram. J. Neurosci. 13 (8), 3266–3283.

Steriade, M., Jones, E.G., McCormick, D.A., 1997. Thalamus. Organisation and Function. Elsevier, Amsterdam, NY.

Stulen, F.B., DeLuca, C.J., 1981. Frequency parameters of the myoelectric signal as a measure of muscle conduction velocity. IEEE Trans. Biomed. Eng. 28 (7), 515–523.

Suffczynski, P., Pijn, J.P.M., Pfurtscheller, G., Lopes da Silva, F.H., 1999. Event-related dynamics of alpha band rhythms: a neuronal network model of focal ERD/surround ERS. In: Pfurtscheller, G., Lopes da Silva, F.H. (Eds.), Handbook of Electroencephalography and Clinical Neurophysiology, Revised Series. Elsevier Science, B.V., Amsterdam, pp. 67–85.

Suffczynski, P., Kalitzin, S., Pfurtscheller, G., Lopes da Silva, F.H., 2001. Computational model of thalamo-cortical networks: dynamical control of alpha rhythms in relation to focal attention. Int. J. Psychophysiol. 43 (1), 25–40.

Thomson, A.M., 1997. Activity dependent properties of synaptic transmission at two classes of connections made by rat neocortical pyramidal neurons in vitro. J. Physiol. 502 (1), 131–147.

Thomson, A.M., West, D.C., Hahn, J., Deuchars, J., 1996. Single axon IPSPs elicited in pyramidal cells by three classes of interneurones in slices of rat neocortex. J. Physiol. 496 (Pt 1), 81–102.

Timofeev, I., Contreras, D., Steriade, M., 1996. Synaptic responsiveness of cortical and thalamic neurones during various phases of slow sleep oscillation in cat. J. Physiol. 494 (Part 1), 265–278.

van Boxtel, A., 2001. Optimal signal bandwidth for the recording of surface EMG activity of facial, jaw, oral, and neck muscles. Psychophysiology 38 (1), 22–34.

van Boxtel, A., Goudswaard, P., van der Molen, G.M., van den Bosch, W.E., 1983. Changes in electromyogram power spectra of facial and jaw-elevator muscles during fatigue. J. Appl. Physiol.: Respiratory, Environ. Exercise Physiol. 54 (1), 51–58.

van Rotterdam, A., Lopes da Silva, F.H., van den Ende, J., Viergever, M.A., Hermans, A.J., 1982. A model of the spatial–temporal characteristics of the alpha rhythm. Bull. Math. Biol. 44 (2), 283–305.

Varela, J.A., Song, S., Turrigiano, G.G., Nelson, S.B., 1999. Differential depression at excitatory and inhibitory synapses in visual cortex. J. Neurosci. 19 (11), 4293–4304.

Wang, X.-J., 1999. Synaptic basis of cortical persistent activity: the importance of NMDA receptors to working memory. J. Neurosci. 19, 9587–9603.

Weese, G.D., Phillips, J.M., Brown, V.J., 1999. Attentional orienting is impaired by unilateral lesions of the thalamic reticular nucleus in the rat. J. Neurosci. 19 (22), 10135–10139.

Williams, J.M., Givens, B., 2003. Stimulation-induced reset of hippocampal theta in the freely performing rat. Hippocampus 13 (1), 109–116.

Williamson, S.J., Kaufman, L., Lu, Z.L., Wang, J.Z., Karron, D., 1997. Study of human occipital alpha rhythm: the alphon hypothesis and alpha suppression. Int. J. Psychophysiol. 26 (1–3), 63–76.

Wilson, H.R., Cowan, J.D., 1973. A mathematical theory of the functional dynamics of cortical and thalamic nervous tissue. Kybernetik 13, 55–80.

Wright, J.J., 2000. Brain dynamics: modeling the whole brain in action. In: Gordon, E. (Ed.), Integrative Neuroscience: "Bringing together Biological Psychological and Clinical Models of the Human Brain". Harwood Academic Publishers, Amsterdam, pp. 139–162.

Wright, J.J., Liley, D.T.J., 1994. A millimetric-scale simulation of electrocortical wave dynamics based on anatomical estimates of cortical synaptic density. Network: Comput. Neural Syst. 5191–201s

Wright, J.J., Liley, D.T.J., 1995. Simulation of electrocortical waves. Biol. Cybern. 72, 347–356.

Yingling, C.D., Skinner, J.E., 1976. Selective regulation of thalamic sensory relay nuclei by nucleus reticularis thalami. Electroencephalogr. Clin. Neurophysiol. 41 (5), 476–482.